A critical review on catalyst design for aqueous phase reforming

Available online at www.sciencedirect.com

ScienceDirect

journal homepage: www.elsevier.com/locate/he

Review Article

A critical review on catalyst design for aqueous phase reforming

Giuseppe Pipitone, Giulia Zoppi, Raffaele Pirone, Samir Bensaid *

Department of Applied Science and Technology, Politecnico di Torino, Corso Duca Degli Abruzzi 24, 10129, Turin, Italy

HIGHLIGHTS

- The research on catalyst design for aqueous phase reforming has been reviewed.
- The effect of preparation method, metal choice and support was evaluated.
- Use of first-principle approaches and in-situ techniques was reported.
- Challenges and perspectives for optimal catalyst system were proposed.

GRAPHICAL ABSTRACT

ARTICLE INFO

Article history:
Received 5 March 2021
Received in revised form
10 September 2021
Accepted 24 September 2021
Available online 29 October 2021

Keywords:
Aqueous phase reforming
Biomass valorization
Biorefinery
Catalyst development
Hydrogen production
Wastewater valorization

ABSTRACT

The aqueous phase reforming (APR) is a catalytic reaction able to produce hydrogen from oxygenated compounds. The catalytic system plays a pivotal role to permit high conversion of the substrate, high selectivity towards hydrogen, and stability in the view of an industrial application. These figures of merit depend on several strategies taken by the researchers to properly design the catalyst, like the preparation method, the choice of the active metal together with possible promoters, the type of the support and so on. The available literature reports several studies where these parameters are evaluated and discussed. In this review, they were critically examined with the aim of finding correlations between the properties of the catalyst and the activity, selectivity and stability for the APR of carbon-laden water fractions. Both theoretical and experimental works have been included in the literature survey. When available, studies with the use of in-situ techniques allowed to increase the understanding of the catalytic phenomena involved in the reaction. Great attention was also reported to recently published works, so that the review could present the most up-to-date developments in the field. The most important outcomes regarding each parameter have been highlighted; moreover, the synergy among each of

* *Corresponding author.*
E-mail address: samir.bensaid@polito.it (S. Bensaid).

https://doi.org/10.1016/j.ijhydene.2021.09.206

them has been pointed out, together with the trade-off that the researcher has to deal with in the pursuit of the optimum catalyst.

Contents

Abbreviation list

APR	Aqueous phase reforming
ATR-IR	Attenuated total reflection-infrared
BE	Binding energy
CO-TPD	CO-Temperature programmed desorption
CO_2-TPD	CO_2-Temperature programmed desorption
DFT	Density functional theory
DRIFTS	Diffuse reflectance infrared Fourier transform spectroscopy
EXAFS	Extended X-ray absorption fine structure
FTIR	Fourier-transform infrared spectroscopy
H_2-TPR	H_2-Temperature programmed reduction
IE	Ionic exchange
IEA	International Energy Agency
IR	Infrared
IWI	Incipient wetness impregnation
MWCNT	Multi walled carbon nanotubes
NH_3-TPD	NH_3- Temperature programmed desorption
PEMFCs	Proton exchange membrane fuel cells
PVP	Polyvinylpyrrolidone
SCS	Solution combustion synthesis
SGA	Sol-gel in acidic conditions
SGB	Sol-gel in basic conditions
SWCNT	Single wall carbon nanotubes
TEM	Transmission electron microscopy
TEOS	Tetraethylorthosilicate
TOF	Turn over frequency
TOS	Time on stream
TPO	Temperature programmed oxidation
UCM	Urea matrix combustion method

WGS	Water gas shift
WHSV	Weight hourly space velocity
XANES	X-ray absorption near edge structure
XAS	X-ray absorption spectroscopy
XPS	X-ray photoelectron spectroscopy
XRD	X-ray diffraction

Introduction

The use of fossil fuels are considered the leading cause of global warming. For this reason, alternative and sustainable sources of energy are explored nowadays to overcome this issue. The use of biomass to substitute fossil oil to produce materials and energy brought to the development of the biorefinery concept. According to the International Energy Agency (IEA) definition, it is intended as the integration of different processes for the sustainable production of goods starting from biomass [1]. One of the advantages of biorefinery is the possibility of targeting small, decentralized plants; as a matter of fact, several drawbacks have been raised for large-scale implementation. One reason is due to the difficulty to reach a complete and effective exploitation of the organic content of the starting biomass. For example, in the biodiesel industry, 1 kg of undesired crude glycerol is produced together with 10 kg of the desired product, generating a considerable amount of waste [2]. Similarly, pyrolysis and hydrothermal liquefaction aim at producing a biofuel (namely bio-oil or bio-crude) [3], but a significant fraction of the carbon present in the feed is lost in the aqueous stream [4].

Aqueous phase reforming (APR) process was proposed by Dumesic and coworkers to valorize oxygenated molecules and obtain a gas mixture rich in hydrogen [5]. It derives that it can be applied to carbon-laden wastewaters present in bio- and conventional refineries to increase the conversion efficiency of the plant, reducing the amount of waste that should be treated, and obtaining at the same time a valuable product. Most of the literature refers to the use of model compounds, such as alcohols (methanol, ethanol), polyalcohols (ethylene glycol, glycerol, xylitol, sorbitol) and represent a pillar of the present review since it focuses mainly on the development of the catalyst. Fewer works have been dedicated to complex matrixes (glucose, xylose, woody biomass) [6,7]. Finally, limited researches described the performance of multicomponent mixtures, close to an industrial application (e.g. wastewater from the brewery industry, food industry) [8–14].

Previous reviews on aqueous phase reforming focused both on the influence of the reaction conditions and the catalytic systems. Davda et al. reported in the first review the fundamentals of their pioneering research [15]. Chen et al. reported the different reaction mechanisms among the substrates [16], while Coronado et al. summarized in their review a large number of issues, helping to compare various parameters [17]. Vaidya et al. classified the available literature on the base of the starting substrate [18]. Finally, very recently, El Doukkali et al. reviewed the research of effective catalysts for the valorization of glycerol through steam reforming, hydrogenolysis and, indeed, APR [19].

Despite most of the works looked at the development of an effective catalyst, this subject has not been comprehensively reviewed so far in the APR field. For this reason, the present work aims to review the actual knowledge on the design of catalytic systems for the valorization of biomass-derived compounds via APR.

Chapter 2 deals with a brief introduction to the process to show its possible applications and advantages. Thermodynamic and kinetic considerations are reported, with a particular focus to the latter, since its knowledge constitutes the basis for the rational design of the catalyst.

The core of the work is based on the effect of different parameters on the performance of the process. The scientific contributions were extensively reviewed, starting from the pioneering works of the Dumesic's research groups up to the most recently published ones.

Chapter 3 outlines the influence of the active site, both in monometallic and bimetallic systems, with specific attention to Pt-based bimetallic systems; moreover, structure sensitivity effects are discussed. Chapter 4 describes the impact of the support's choice on the APR performance. Chapter 5 deals with the effect of the preparation method as a key step for determining the properties of the catalyst and, in turn, the yield of the desired product. The open questions and challenges related to catalytic and technological subjects are discussed in Chapter 6.

The research papers have been classified in the corresponding chapter according to the main aim of the study, although defining proper boundaries is not trivial. For example, bimetallic catalysts can alter both electronic properties (modifying the bond strength of reactants, intermediates and products) and structural properties (modifying the dispersion and, consequently, the number of available sites).

Throughout the review, specific attention is put to the use of density functional theory (DFT), microkinetic modelling or in situ techniques to get information for the design of new catalysts. In fact, since the catalyst structure can be modified by the environment during the reaction itself, in situ characterizations can inspect connections between the catalyst structure and its performance. In conclusion, the primary outcomes are summarized and integrated to have some final messages for the design of an active, selective, and stable APR catalyst.

Fundamentals of aqueous phase reforming

The aqueous phase reforming is a process carried out at mild temperatures (220–270 °C) and pressures (30–60 bar), in the presence of a catalyst [15]. In these conditions, the aqueous solution remains in the liquid phase, leading to an energetic advantage thanks to the avoided vaporization. This is one of

the potential benefits of APR compared to the conventional steam reforming process, that is performed typically at about 800 °C. The reaction stoichiometry is reported in equation (1).

$$C_nH_{2y}O_n \leftrightarrow nCO + yH_2 \quad (1)$$

In Fig. 1, the influence of temperature on the Gibbs free energy for the reforming of alkanes and alcohols is reported. It can be observed that oxygenated hydrocarbons have a more favorable equilibrium, i.e., the hydrogen production can occur at lower temperatures than if obtained from alkanes.

In the same temperature range, the water gas shift (WGS) reaction is favored as well (equation (2)).

$$CO + H_2O \leftrightarrow CO_2 + H_2 \quad (2)$$

This occurrence allows to generate in one reactor a gas mixture where CO is present in negligible percentage, making the gas stream a compatible feed for low temperature proton exchange membrane fuel cells (PEMFCs); contrarily, in the steam reforming plant, a double configuration with high- and low-temperature water gas shift reactors is necessary to maximize the hydrogen yield.

Combining equations (1) and (2) we can derive the conventional reaction stoichiometry for APR (equation (3))

$$C_nH_{2y}O_n + nH_2O \leftrightarrow nCO_2 + (y+n)H_2 \quad (3)$$

It is important to recall here that, despite the advantageous thermodynamics for hydrogen production, another reaction involving hydrogen consumption is more favored: the methanation reaction (equation (4)).

$$CO_2 + 4H_2 \leftrightarrow CH_4 + 2H_2O \quad (4)$$

The APR mechanism is constituted by different steps, in which the interactions of the molecule with the active site, the support and their interface play a fundamental role to determine the product distribution. Knowing the possible steps involving the reacting molecule is essential to properly design the catalyst, tuning its structural, morphological, and textural properties to favor one pathway rather than the other. The possible reaction mechanism of glycerol APR is described in Fig. 2. As will be reported in the next paragraphs, glycerol was chosen as model compound for several works, due to the importance of its valorization for the biodiesel value chain.

The substrate can undergo dehydration (a) with the acid sites of the support, leading to hydroxyacetone, which can be subsequently hydrogenated (b) to propylene glycol. This route is undesired because hydrogen is consumed.

If the molecule interacts with the metal active site, it is generally agreed that the dehydrogenation (c) of the molecule is the first step (glyceraldehyde intermediate). Afterwards, it can follow two routes. C–O bond breaking (d) can occur, leading to the formation of alkanes. In this case, since the C–H activation of alkanes is thermodynamically hindered at typical APR temperatures, their hydrogen content cannot be exploited. On the other hand, C–C bond breaking (e) can lead to the formation of carbon monoxide. This intermediate, while adsorbed on the active site, may interact with water that, once catalytically activated (i.e., $H_2O \rightarrow OH + H$), produces hydrogen and carbon dioxide via WGS (f). Another

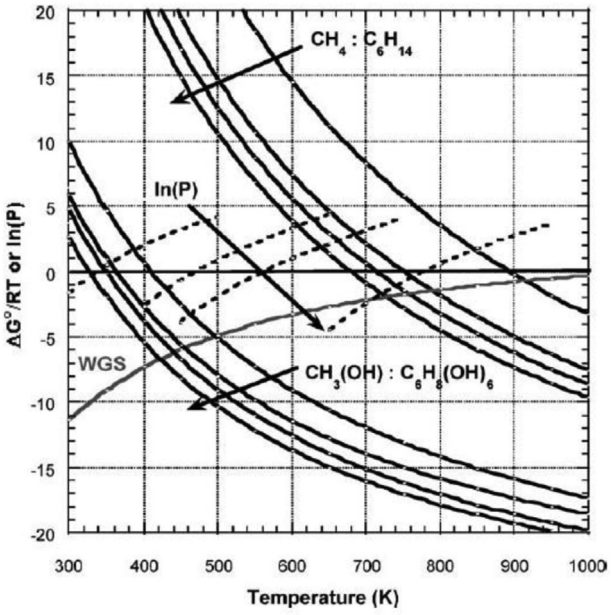

Fig. 1 – Gibbs free energy for vapor-phase reforming of small alkanes and alcohols, water gas shift, and vapor pressure of alcohols in dotted lines (from Ref. [15]).

detrimental route is that CO undergoes methanation (or Fischer-Tropsch reaction), consuming hydrogen (g).

Taking into consideration the reported possible reaction pathways, some key points should be considered by the catalyst designer to maximize the hydrogen production:

- Dehydrogenation, C–C bond breaking, H_2O activation, and water gas shift reaction should be favored;
- C–O bond breaking, methanation/Fischer-Tropsch and dehydration should be avoided.

As graphically reported in Fig. 3, preparing the catalyst involves three main choices regarding the preparation, the metal and the support. In the next chapters, the available literature will be presented with the aim of systematically pointing out how each of these choices can be beneficial or detrimental to the activation of each of the reported steps, i.e., favor C–C bond breaking more than C–O breaking, or activate water dissociation without worsening the support stability. APR is strongly sensitive to the reaction conditions, such as nature and concentration of the feed, reaction temperature and pressure, catalyst amount, reactor configuration. It derives that fair comparisons of results between different works are difficult and will be limited in this review.

Effect of the metal

In the present chapter, the effect of the active metal is reported. At the beginning, a comparison between monometallic systems is performed, both using first-principles and experimental methods. Afterwards, the synergy of bimetallic catalysts is reported, with a higher attention to Pt-based and Ni-based formulations. Specific paragraphs are dedicated to

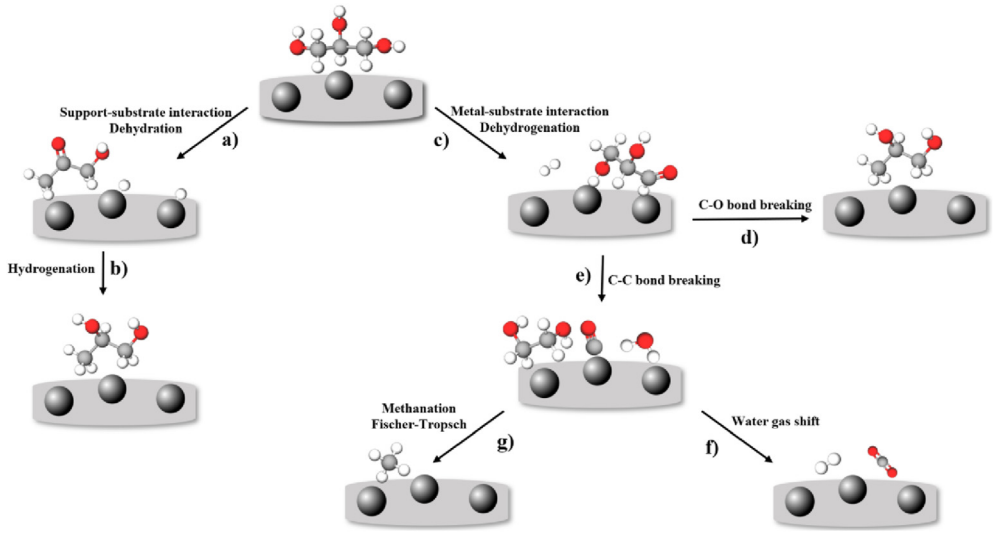

Fig. 2 – Reaction mechanism for glycerol aqueous phase reforming.

systems considered particularly interesting both for the obtained results and for the extent of characterization (i.e., Pt–Mo, Pt–Co, Pt–Ni, Pt–Re, Ni–Cu). Finally, the influence of the particle size is discussed.

Monometallic systems

Platinum is the most studied metal for aqueous phase reforming since it combines high activity and moderate selectivity. These results have been primarily explained by several DFT investigations. Davda et al. studied the C–C and C–O bond cleavages of ethanol by DFT on Pt [20]. Firstly, the authors reported that Pt–C bonds are more stable than Pt–O bonds examining the stability of different isomeric species. Secondly, they suggested that the C–C bond cleavage should be faster than the C–O bond cleavage because the energy for the transition state of the former is one order of magnitude lower than the latter (4 vs 42 kJ/mol) [21]. It follows that, recalling Fig. 2, path e) is more favored than path d).

In Fig. 4 the possible steps involved in ethanol reforming on Pt are depicted [22]. After being adsorbed on the active site, ethanol can follow two routes for the first dehydrogenation

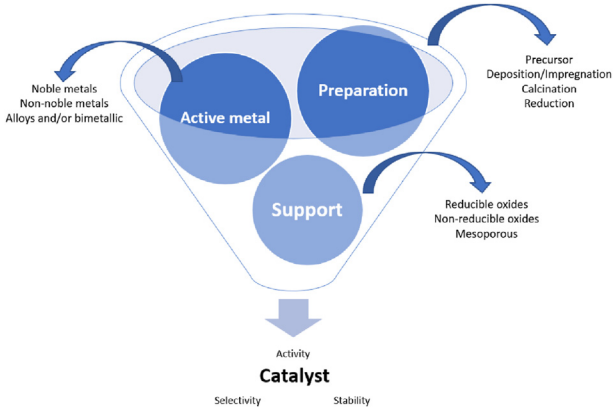

Fig. 3 – Design funnel of heterogeneous catalyst.

according to which H is abstracted (ethoxy CH_3CH_2O or 1-hydroxyethyl CH_3CHOH); in the second step, this intermediate is dehydrogenated in acetaldehyde. Thereafter, the adsorbed acetaldehyde further dehydrogenates into acetyl (CH_3CO), ketene (CH_2CO) and ketenyl (CHCO) (please note that only the most plausible species were reported here among the possible pathways). It is just the ketenyl species that finally is subjected to C–C bond breaking to CO and methylidyne (experimentally confirmed). This outcome has been compared in a proper work in which DFT, microkinetic investigation and experiments have been combined [23]. The authors observed that the level of hydrogenation of the intermediates influenced the C–C or C–O cleavage barriers because of geometric and electronic effects. In this sense, more dehydrogenated species facilitated C–C bond breaking having the C–C bond parallel to the surface. The microkinetic model also highlighted that the formation of 1-hydroxyethyl via α C–H scission (CH_3CHOH) is predominant compared to CH_3CH_2O after first ethanol dehydrogenation (bold arrows in the corresponding figure). Further theoretical works on platinum with different substrates were reported in Refs. [24–26], attaining analogous conclusions.

On ruthenium, the activation energy for C–C bond cleavage is lower than on platinum, being 38 kJ/mol when the surface CH_2CO species is formed (while it is 90.24 kJ/mol on Pt after CHCO), so it is more sensitive to the first dehydrogenation steps [27]. However, it is far more active towards methanation than Pt, decreasing the hydrogen selectivity [28].

The decomposition of glycerol has been explored also on Pd, Rh, Cu, Ni, focusing on dehydrogenation, C–C and C–O cleavage [29]. Glycerol binds similarly on Pt, Pd, Rh, Cu, through the hydroxyl groups. The four possible monodehydrogenated species are reported, derived from C–H or O–H cleavage of the terminal or central carbon. Furthermore, the binding energies related to more dehydrogenated intermediates and C–O cleavage are reported as well. In agreement with previous studies, it has been reported that C–C breaking is favorable on Pt after several dehydrogenation steps, and it is more facile than C–O breaking. Despite the

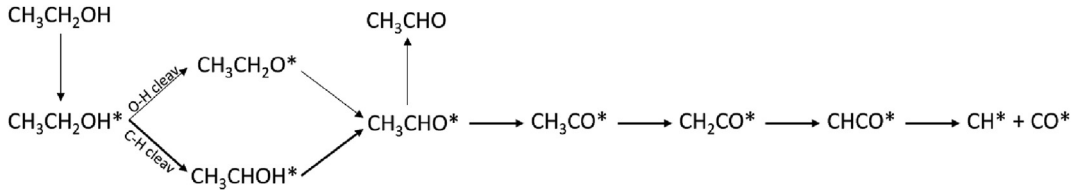

Fig. 4 – Most plausible decomposition pathway of ethanol on Pt (111). Adapted with permission from Ref. [23]. Copyright 2013 American Chemical Society.

simplification of the models, the results were coherent with the experimental outcome. The pathway is similar on Pd, i.e., dehydrogenation up to $C_3H_5O_3$ is necessary and C–C is more favorable, but the lowest C–C scission transition state energy is higher than on Pt, suggesting that Pt is more active. Despite dehydrogenation is always necessary, the situation is different on Rh and Ni, where the energies between C–C and C–O are more comparable. Moreover, the transition states are quite low in terms of activation energy, explaining the experimentally known high activity of Ni despite its low selectivity. Finally, on Cu the transition states show a quite high activation energy, highlighting the low Cu activity. It is worthy to point out that the model was further implemented considering the presence of adsorbed CO. Higher coverage of CO increased the free energy for glycerol dehydrogenation, emphasizing the pivotal role of the water gas shift reaction in the process to reduce the concentration of adsorbed CO.

Davda et al. initially experimentally investigated Pt, Ni, Ru, Rh, Pd and Ir supported on silica for ethylene glycol APR [30]. In their kinetic study, the authors reported the promising ability of Pt to produce hydrogen, while Pd showed low activity and the highest selectivity (Fig. 5). Looking at non-noble metals, Ni was comparable to Pd, but suffered from low selectivity (alkane production) and it was more prone to deactivation. The use of a cheap material, such as Ni, would increase the cost-effectiveness of the process. However, its low stability and H_2 TOF (ten-fold lower than platinum) would impede its utilization in a larger scale context.

Bimetallic systems: a short introduction

It has been largely reported that bimetallic catalysts perform better than monometallic in many different fields, and APR is part of this family [31]. Before entering in the core of the paragraph, it is worthy to cite the first outcomes derived from the works carried out in the Dumesic's research group.

Huber et al. used a high-throughput system to study several catalyst formulations for ethylene glycol APR [32]. They found that Sn addition to Raney Ni catalyst greatly improved its performance. Sn was mainly present at Ni defect-sites and as an alloy (e.g. Ni_3Sn), without affecting the Ni particle size. In this way, Sn hindered the CO methanation that, over Ni catalysts, preferentially occurs in the defects. This outcome was further explored in successive works. The addition of Sn, Au or Zn to Ni/alumina catalyst promoted the hydrogen selectivity, with Sn being the best promoter [33]. Being alumina not stable, Sn was added to Raney-Ni catalysts. With only 400:1 Ni:Sn atomic ratio, the methane production was halved, and eliminated at 18:1. The modified catalyst deactivated in the first 48 h by sintering, and afterwards by re-oxidation of the active site because of the interaction with water (no coke). Leaching of Ni was explained by formation of organometallic species after interaction of the catalyst with the feed. This phenomenon was reduced as well thanks to Sn addition. Finally, since Pt and Pd showed the best performance in monometallic systems, more than 130 Pt and Pd bimetallic catalysts based on these noble metals were screened using APR of ethylene glycol as probe reaction [34]. Four bimetallic catalysts were particularly interesting for their results: Pt–Ni, Pt–Co, Pt–Fe and Pd–Fe. The authors reported that alloying Pt with Ni, Co and Fe led to an electronic modification of Pt which caused the decrease in the binding energy (BE) of hydrogen and carbon monoxide and the increase in the dissociative adsorption energy of hydrogen. On the other hand, Fe addition in Pd-based catalyst promoted the WGS, which is considered the rate determining step on monometallic Pd.

The next paragraphs report the outcome of several bimetallic systems, including the motivation that the authors proposed to explain the structure-activity relationship. The huge amount of information required a strong effort to rationalize and understand how to present it. They were not reported chronologically; rather, it was in the aim of the authors give a progressive insight into the phenomena, collecting different researches on similar systems to have common outputs. The paragraphs are divided according to the main actor of the system, e.g. platinum, nickel, etc., despite some of them could have been reported in more than one paragraph

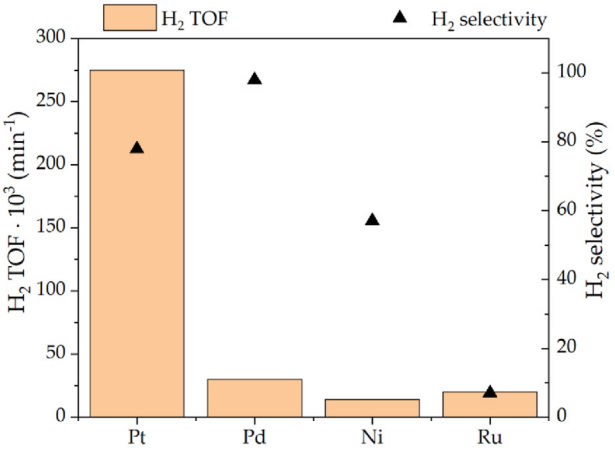

Fig. 5 – APR of ethylene glycol. Reaction conditions: 225 °C/22 bar, 10 wt% ethylene glycol solution, 0.06 mL/min (data from Ref. [30]).

(i.e., the description of Pt–Ni could have been stated in the Pt or Ni section). Finally, ad hoc sub-paragraphs were dedicated to the most interesting Pt-based (Pt–Co, Pt–Mo, Pt–Ni, Pt–Re) and Ni-based (Ni–Cu) systems in order to go deeper with their comprehension. If not clearly stated, glycerol is considered as the feedstock.

Pt-based catalysts

Godina et al. investigated the APR of xylitol over mono and bimetallic catalysts [35]. Among the platinum-based bimetallic catalysts, Pt–Re showed the highest conversion at each weight hourly space velocity (WHSV) investigated (Fig. 6-A). This outcome was related to the higher water gas shift, promoted by Re. Low amount of erythritol was found in the liquid phase, suggesting that C–O cleavage was favored over C–C. Pt led mainly to propane, being active for C–C, while Pt–Re mostly led to butane and propane. Overall, because of the lower hydrogen selectivity of the bimetallic system than the monometallic one, the hydrogen turnover frequency of the former was lower than the latter (about 23 min^{-1} vs 26 min^{-1}, at WHSV 9.5 h^{-1}).

Larimi et al. investigated different promoters (Rh, Cr, Re, Pd, Ru, Ir) for Pt-based catalysts supported on γ-alumina [36]. As reported in Fig. 6-B, while the conversion was approximately constant (about 82%), the hydrogen selectivity was minimum for monometallic Pt (69.9%) and maximum for Pt–Rh (89%). The variation of the lattice constant proved the formation of a solid solution. It was suggested that Rh helped the WGS, at the same time increasing the mobility and reactivity of surface oxygen atoms. The benefic addition of Rh was also reported in Ref. [37], where the use of MgO-supported nano-sheet catalysts allowed stability during 100 h TOS (time on stream), overcoming the limitations reported by Ref. [38].

The addition of Rh can have different effects on different supports. When added to Pt/α-alumina, both the hydrogen yield and the stability increased, by preventing coke formation favoring methanation [39]. On the other hand, Pt/γ-alumina's performance was negatively influenced by Rh, with a slight decrease of the hydrogen yield and catalyst life span (46.3 h vs. 51.6 h).

Guo et al. investigated the APR of glycerol on different Pt-based bimetallic catalysts [40]. The alloys were pre-synthesized and successively loaded on the support (γ-Al_2O_3) to exclude the influence of the particle size. Among the promoters (Ni, Co, Fe, Cu), Fe showed the highest carbon conversion to gas and hydrogen yield, with 1:1 considered as optimal atomic ratio. Water gas shift tests showed consistent results with the APR tests. The coherent results between APR and WGS confirmed that the latter has a strong influence on the overall result. To further investigate this aspect, in situ diffuse reflectance infrared Fourier transform spectroscopy (DRIFTS) was utilized. It was showed that formate desorption is not easy on Pt/alumina, while it was easier for the Pt–Fe system. It was suggested that Fe promoted the water activation producing OH groups that can react with the proximate CO adsorbate on Pt. This is the reason why 1:1 atomic ratio led to the best results, because it is the one which presented the highest proximity between the two metals. Moreover, it favored the formate decomposition that causes otherwise the sites blocking. Further works on Pt–Fe bimetallic systems were reported in Refs. [41,42]. Moreover, further DRIFTS spectra showed new CO adsorption sites on Fe in Ref. [43].

Dosso et al. studied bimetallic Pt based catalysts promoted with Ni or Co for APR of polyols derived from glucose degradation [44]. Pt and Ni are completely miscible, and this occurrence affected the electronic properties of Pt reducing the binding of adsorbate. This is in agreement with the results reported in Ref. [34]. X-ray photoelectron spectroscopy (XPS) showed that Pt was mainly in the oxidized state (Fig. 7-A), likely because of the donation of electrons. The interaction of Pt with Co and Ni was suggested by the presence of a broad peak of reduction in the H_2-TPR, as depicted in Fig. 7-B. Pt–Ni showed higher yield than Pt–Co. No direct comparison with the monometallic could be performed as the authors used also different preparation techniques, namely urea matrix combustion method (UCM) and incipient wetness impregnation (IWI). Being Ni not active for water gas shift, a high selectivity to CO was observed (almost 20-fold the one of Pt–Co). The authors finally highlighted the higher presence of coke on Pt–Ni compared to Pt–Co, not directly explained by its limited higher activity.

Pendem et al. studied the effect of potassium promotion on Pt/Hydrotalcite catalysts for APR of glycerol [45]. Despite potassium addition decreased the surface area, it contributed to the increase of the surface basicity (measured by CO_2-TPD) and stabilizing the Pt precursor, increasing the final dispersion of the active site. Adding 2.8% of K increased the glycerol conversion from 27 to 88%. Further addition up to 16.9% K decreased the activity likely for the covering of Pt particles (67% conversion). However, increasing the loading up to 28% changed the morphology improving further the dispersion and allowing to reach 83% conversion. Moreover, the increase of basicity caused an increase in the H_2 selectivity. Finally, the catalyst showed stable performance after four runs, without appreciable leaching of both Pt and K. The effect of a second metal in modifying the acid-base properties of the catalyst was also reported in Ref. [46] for Mn. The results were comparable with [47] in the case of ethylene glycol APR, despite no leaching was observed in this case.

Another way to improve the APR performance was reported adding Ru to Pt-based catalysts on carbon supports prepared by impregnation [48]. In the APR of wheat straw hydrolysate, Pt–Ru/Multi walled carbon nanotubes (MWCNT) showed the highest activity and hydrogen selectivity. It was attributed to the electron donor effect of Ru that increased the Pt electron density, filling its d-band and reducing the strength of adsorption of organics. The proximity of Ru and Pt clusters was the key to enhance the catalysis. In fact, the same did not happen using a different support, activated carbon. In this case, the catalyst was constituted by unpaired Pt and Ru atoms, which consequently were unable to express their synergy.

Despite not performed in the context of APR, it is interesting to cite here that the addition of Ru improved also the sulfur tolerance of Pt monometallic [49]. The authors exploited the sulfur spillover concept, due to the higher resistance of ruthenium, and the hydrogen spillover that can regenerate the catalyst. Extended X-ray absorption fine structure (EXAFS) determination of the coordination number showed the

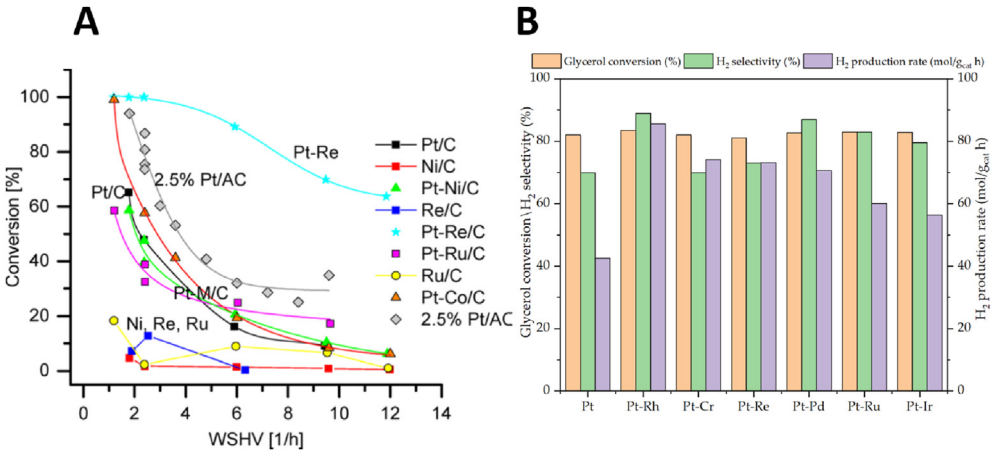

Fig. 6 – A: Influence of WHSV on xylitol conversion for different carbon-supported mono and bimetallic catalysts. Reaction conditions: 225 °C/29.7 bar, 0.5 g catalyst, 100 g/l xylitol (from Ref. [35] - https://pubs.acs.org/doi/10.1021/acs.iecr.7b04937 - further permissions should be directed to the ACS); B: Performance of Pt-based catalyst with different promoters. Reaction conditions: 250 °C/50 bar, 0.25 g catalyst, WHSV 2.45 h^{-1} (data from Ref. [36]).

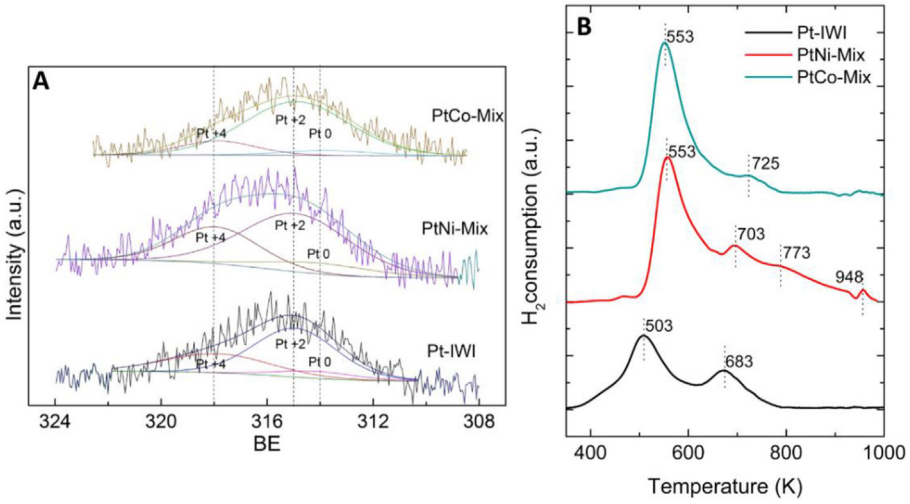

Fig. 7 – A: XPS spectrum in the Pt $4d_{5/2}$ zone and B: H_2-TPR of the reduced catalysts. "Mix" in the bimetallic system refers to the preparation method of the bimetallic catalyst, i.e., IWI for Pt incorporation and UCM for Ni and Co dispersion. From Ref. [44].

presence of an alloy at the three investigated ratios (Fig. 8 - step 1). Sulfur species may interact with platinum (step 2) and then move to Ru by spillover (step 3), or directly interact with the latter (step 4). The authors reported that sulfur poisoning caused dealloying; afterwards, hydrogen spillover (step 5) could allow the removal of sulfur. Indeed, the regenerated sample showed similar spectra than the fresh one, through a re-alloying mechanism. In this sense, the atomic balance between the two metals is fundamental to favor both the sulfur-trap capacity (given by Ru) and the spillover at proximity.

The last example reported in the paragraph regards the use of Zn as promoter. Lei et al. used atomic layer deposition to modify Pt/alumina catalysts by ZnO promotion [50]. A higher hydrogen production was obtained when Pt was deposited before than Zn. This is because it took advantage of the two interfaces Pt–ZnO and Pt–Al_2O_3. Thanks to X-ray absorption near edge structure (XANES) spectroscopy, the authors suggested that the significant charge transfer from Zn to Pt promoted the H_2 selectivity. Moreover, the bimetallic system showed only limited sintering (the particle size increased from 0.9 nm to 1.2 nm), contrarily to the monometallic catalyst (from 1.0 nm to 2.4 nm).

Table 1 summarizes the effects of the cited promoters on the performance of APR when added to Pt-based catalysts. It can be observed that the positive impact is commonly associated to the promotion of water gas shift, which can be obtained by different paths (increase of surface basicity, water activation, easier intermediates desorption). One typical drawback is that the increase of the conversion is (partially) counterbalanced by the decrease of the hydrogen selectivity, since methanation is promoted as well. It is important to observe that in some cases different results were obtained, despite similar catalytic systems and analogous substrates were used, such in the case of Pt–Rh on gamma alumina

([37,39]), or for Pt-Mn ([46,47]). On the other hand, similar results were obtained also with different substrates such as ethylene glycol or glycerol for Pt-Fe ([34,40]), or three different polyols in the case of Pt-Co ([44]).

Platinum–molybdenum

Dietrich et al. studied a Pt–Mo bimetallic catalyst supported on carbon prepared by IWI [51]. Transmission electron microscopy (TEM) showed that the bimetallic nanoparticles sintered during glycerol reforming, with the average size moving from 2 nm to 5.1 nm. X-ray absorption spectroscopy (XAS) showed that the Pt–Mo nanoparticles are metallic Pt-rich with the presence of Mo in different states (metallic when close to Pt, oxide when in isolated clusters, as reported in Fig. 9-A). Even more interesting, operando XAS was carried out to evaluate if the state of the catalyst changes during the reaction. It was reported that Pt remained in the metallic state and its coordination number increased, coherently with the results reported by TEM. Overall, the basic structure remained the same, with a Pt-rich core and Mo in the near surface region of the nanoparticle. This is coherent with DFT calculations which predicts an analogous core-shell composition when starting from metallic Pt and MoO precursors.

The comparison with monometallics and the extensive study on the role of Mo using operando spectroscopy and DFT was performed in a following work [52]. The authors reported that Pt was the real active site, while Mo acted as a promoter modifying the electronic properties of Pt and its interaction with the adsorbed molecules. DFT calculations showed that Mo decreased the Pt–CO binding energy; as a matter of fact, XANES showed that CO was the most abundant surface species in the case of Pt/C (about 0.6 fractional coverage), while it was under the detection limit for Pt–Mo/C. At the same time, it reduced the kinetic barrier for dehydrogenation and even more for C–O bond cleavage, leading globally to a reduction of the H_2 selectivity (Fig. 9-B). Further DFT investigations in agreement with the ones reported here can be found in Ref. [53], where the role of Mo oxide is highlighted regarding the change of WGS mechanism and the bifunctionality of the catalytic system is suggested.

Platinum–cobalt

The promotion of Co was studied on Pt supported on MWCNT by IWI [54]. Co raised by 4.6 times the glycerol activity normalized per Pt surface. The improvement was ascribed to the WGS promotion, so by removing the strong CO adsorbed on the Pt site facilitating the water activation. The hydrogen selectivity slightly increased compared to the monometallic Pt, in the whole range of glycerol conversion (Fig. 10-A). Pt–Co and Pt showed an increase of the particle size from 1 nm to 2 nm (more than one-week test), indicating a good stability of the catalytic system. Pt–Co particles were found in three different configurations: Pt clusters (59%), Co core – Pt shell (30%) and Pt–Co alloy (11%). Therefore, despite only 40% of the particles was in the bimetallic form, still the performance improved. The high presence of Pt on the surface, contrarily to the case of the Pt–Mo where it was in the core, may explain the maintenance of high hydrogen selectivity. XANES outcome reported a downward shift in the d-band center compared to the monometallic Pt, which is related to a lower binding energy of CO.

The same research group further evaluated the effect of Co addition to Pt-based catalysts performing operando X-ray absorption spectroscopy (XAS) investigation [55]. Adding Co increased the site time yield up to four-fold when the catalyst composition was 1Pt5Co (i.e., 1:5 Pt-to-Co molar ratio). Please note that monometallic Co showed negligible activity. The comparison between fresh and operando structures of the catalyst exhibited modification because of the hydrothermal environment, despite preserving the bimetallic configuration. The formation of an alloy was considered the reason for the improvement in the performance, rather than the nature of the particles (e.g. Pt shell/Co core). Being maintained the selectivity, the authors suggested that the role of Co was to exalt the Pt properties, at the same time reducing the CO binding energy and improving the WGS.

Previously Wang et al. investigated by XAS Pt–Co nano-alloyed particle systems supported on single wall carbon nanotubes (SWCNT) [56]. XAS spectra showed a core (Co) and shell (Pt–Co) structure, which greatly enhanced the activity without decreasing the selectivity. The electron transfer from Co to Pt may perturbate the latter, probably affecting the reaction path.

Co promotion on Pt based catalysts was also studied on CeO_2–ZrO_2 mixed oxides supports for ethylene glycol APR [57]. As reported in Fig. 10-B, the optimal Co:Pt molar ratio in terms of APR activity and WGS (CO conversion) was found equal to 0.5. The authors suggested that the oxophilic properties of cobalt favored the WGS and penalized the formation of coke (likely hindering acetic acid intermediate formation [58]). Further increase of Co loading decreased the ethylene glycol conversion. The interaction between the two metals was investigated via TPR. Adding the promoter, the strong metal-support interaction Pt–CeO_2ZrO_2 decreased. Other phenomena such as the formation of surface defects and higher dispersion of the bimetallic can contribute to the higher activity. As a matter of fact, the activity trend followed the results of the CO chemisorption. The promoter helped also to stabilize the platinum particles, which were less aggregated in the bimetallic catalyst compared than the monometallic.

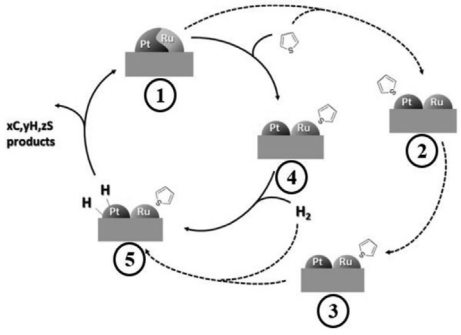

Fig. 8 – Scheme of the in-situ catalyst self-regeneration with thiophene as model compound. Modified from Ref. [49].

Platinum–nickel

Platinum and nickel are likely the most studied active metals for APR, since they can be defined as representatives of two classes. Platinum is the most effective monometallic catalyst,

Table 1 – Summary of the influence of the promoters on Pt-based catalysts for APR.

Catalytic system	Main modifications caused by the promoter	Major drawbacks and unsolved issues	Reference
Pt–Rh	Activity similar to the monometallic; improvement of H_2 selectivity thanks to WGS promotion, increase of Pt reducibility and mobility/reactivity of surface oxygen atoms	Stability issues when crude glycerol was used	[36]
	Higher glycerol conversion and selectivity than the monometallic thanks to higher oxygen mobility which enhanced WGS rate		[37]
	Higher stability and activity by preventing coke formation (on α-alumina support)	Lower selectivity due to methanation promotion; lower activity (on γ-Al_2O_3)	[39]
Pt–Fe	Higher conversion thanks to decrease of CO and H_2 interaction strength with the surface increasing the availability of catalytic sites	Lower selectivity than the monometallic	[34]
	Increase of the H_2 yield thanks to WGS promotion (easier formate desorption and water activation)		[40–43]
Pt–K	Increase of conversion and selectivity thanks to increase of surface basicity and Pt dispersion	Excess of K (>28% loading) blocked Pt species reducing conversion and H_2 selectivity	[45]
Pt–Mn	Moderate increase of conversion and selectivity	Strong Mn leaching under working conditions	[46]
	Increase of conversion and selectivity thanks to alloy formation, increasing Pt reducibility and more favorable WGS		[47]
Pt–Ru	Higher activity and hydrogen selectivity thanks to electron-donor effects which reduced the organics adsorption strengths (on MWCNT)		[48]
	Higher sulfur stability thanks to spillover mechanisms	Close Ru and Pt proximity is required (e.g. same lattice), as well as reducing treatment to recreate the alloy	[49]
Pt–Zn	Increase of H_2 selectivity thanks to charge transfer from Zn to Pt; slighter sintering		[50]
Pt–Mo	Higher H_2 TOF than monometallic thanks to decreased CO interaction strength (increasing the availability of catalytic sites and promoting WGS) and dehydrogenation activation energy	Lower selectivity since C–O cleaving activation energy is lowered	[52,53]
Pt–Co	Higher conversion thanks to decrease of CO and H_2 interaction strength with the surface increasing the availability of catalytic sites		[34]
	Higher H_2 TOF than monometallic since Co alloying decreased CO and H_2 interaction strength with the surface increasing the availability of catalytic sites; Lower methanation selectivity	Higher coke formation than the monometallic	[44]
	Higher H_2 formation thanks to WGS promotion due to Pt–CO binding energy reduction	Only 40% of the particles in the bimetallic form	[54,55]
	Higher H_2 formation thanks to higher Pt dispersion and Pt electronic perturbation		[56]
	Higher activity thanks to WGS promotion and higher dispersion Higher resistance to sintering and lower coke formation		[57]
Pt–Ni	Higher conversion thanks to decrease of CO and H_2 interaction strength with the surface increasing the availability of catalytic sites	Higher alkane selectivity at higher Ni loading	[34]
	Higher H_2 TOF than monometallic since Ni alloying decreased CO and H_2 interaction strength with the surface increasing the availability of catalytic sites	Higher CO selectivity and methanation since WGS is not favored; higher coke formation	[44]
	Higher substrate conversion thanks to higher dispersion	Higher methanation	[59]
	Higher activity and H_2 selectivity thanks to lower H_2 and CO interaction strength, improvement of WGS and higher Pt dispersion Lower coke deposition compared to monometallic	Slight sintering	[60]
	Higher H_2 TOF than monometallic thanks to higher dehydrogenation rate	Sintering of Pt–Ni nanoparticles	[61,62]
Pt–Re	Higher xylitol conversion thanks to WGS promotion	Lower selectivity due to C–O cleavage promotion; no info on the stability	[35]
	Higher H_2 TOF thanks to the decrease of CO strength with the surface increasing the availability of catalytic sites and WGS promotion	Decrease H_2 selectivity due to acidic ReOx (dehydration favored)	[66]
	Higher activity thanks to the promotion of water activation	Decrease H_2 selectivity due to acidic ReOx (dehydration favored)	[68]
	Higher substrate conversion	Decrease H_2 selectivity due to acidic ReOx (dehydration favored)	[69–71]

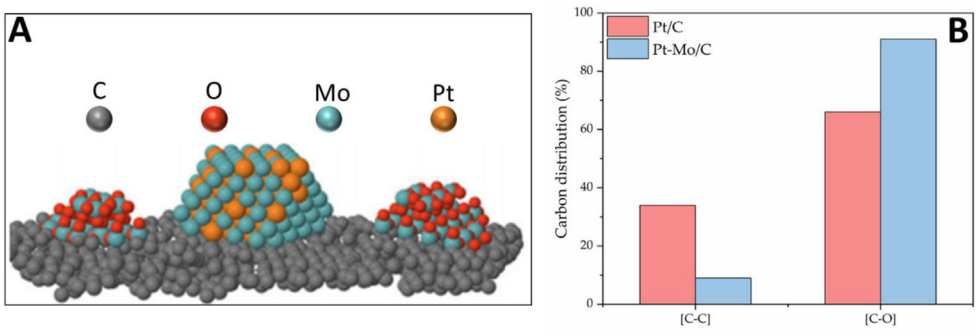

Fig. 9 – A: Proposed PtMo/C structure derived from catalyst characterization (modified from Ref. [51]); B: Carbon conversion of Pt/C and Pt–Mo/C, reaction conditions: 230 °C/30 bar, 30 wt% glycerol solution (data from Ref. [52]).

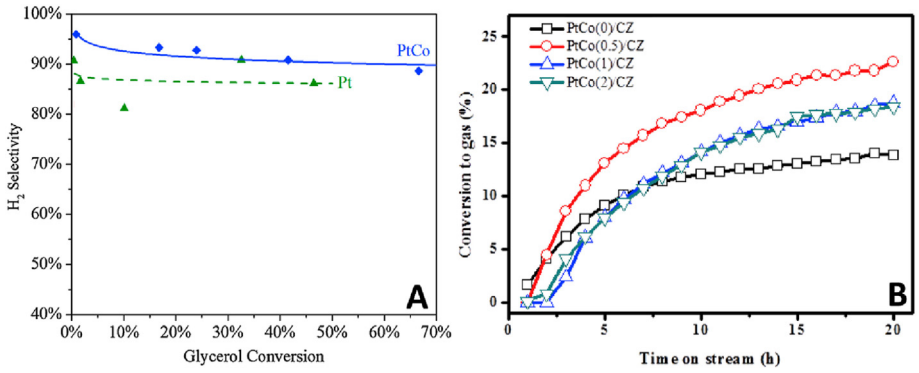

Fig. 10 – A: Influence of glycerol conversion on H_2 selectivity for Pt and PtCo catalyst, reaction conditions: 230 °C/32 bar, 30 wt% glycerol solution (modified from Ref. [54]); B: Influence of Pt:Co molar ratio on conversion of ethylene glycol to gaseous products, reaction conditions: 250 °C/45 bar, space velocity 2 h^{-1} (from Ref. [57]).

but it suffers from a high cost; on the other hand, nickel is cheaper, and despite its performance are less enthusiastic than platinum, its use would increase the cost-effectiveness of the process. Ni/C exhibited much lower activity than Pt/C, particularly at low WHSV, and deactivated rapidly because of Ni leaching during APR of xylitol [35]. Even for Ni-based systems, as will be shown more extensively later, the addition of a promoter improves the performance. For example, it was cited that the presence of Sn in a Raney Ni catalyst led to a hydrogen production per unit volume equal to 350 μmol H_2/cm^3, comparable to the value obtained by Pt/Al_2O_3 (450 μmol H_2/cm^3) [32]. For this reason, several researchers investigated bimetallic systems which involved these two metals.

He et al. studied the optimal ratio between Pt and Ni on MWCNT prepared by IWI for glycerol APR [59]. Adding the second metal allowed to increase the dispersion of Pt. The formation of Pt–Ni alloy modified the electronic properties of Pt, increasing the interaction with the support and thus the dispersion. Adding Ni also caused the highest increase of glycerol conversion (from 26% to 81%), while the carbon conversion approximately increased from 8% to 15% (Fig. 11-A). The hydrogen yield increased from 1.83 mmol H_2/g glycerol for the monometallic to a maximum 2.43 mmol H_2/g glycerol, together with a strong increase of methane (approximately 3 folds higher). This is coherent with the known methanation activity of Ni. Looking at the effect of Ni loading, it was reported that 1:1 was the optimal atomic ratio, since excessive Ni may not form an alloy with Pt and rather cover it.

Different Pt:Ni ratios (1% Pt and 3–18% Ni) on ceria doped alumina catalysts were also investigated in Ref. [60]. Two different types of surface alloys, NiPt and Ni_3Pt, were identified. Adding Ni up to 6% reduced the crystallite size causing the highest activity (96% conversion) and H_2 selectivity (approximately 83%), as depicted in Fig. 11-B. The shift in the Pt $4f_{7/2}$ XPS peaks highlighted the modification of the electronic environment by Ni addition. The synergy between the two metals is proved by the fact that physical mixture of the two catalysts did not perform similarly well. The improvement compared to monometallic Pt was referred to the improvement of WGS thanks to Ni addition, higher dispersion, and lower H_2 and CO binding energy on Pt, making the sites more available. Looking at the catalyst stability, the authors showed that monometallic Ni severely deactivated (metal oxidation, carbon deposition and leaching), while 1Pt6Ni was stable on 85 h TOS (small particles aggregation but not carbon deposition was observed).

Possible structural modification of bimetallic Pt–Ni catalysts under APR conditions were followed thanks to in situ EXAFS analysis [61]. Fig. 11-C shows the modification subjected by the Pt–Ni clusters under APR. When the catalyst is reduced, the core is Ni-rich, while the shell is Pt-rich. However, under APR conditions, the Ni–Pt particles restructures,

with platinum diffusing to the core while Ni segregates to the surface. Importantly, this behavior was reversible prior subsequent re-reduction. The enhanced activity of the bimetallic catalyst compared to monometallic Pt was explained by this segregation. This is coherent with DFT studies which showed higher activity of Ni-terminated (i.e., Ni-rich surface) Pt–Ni nanoparticles due to the increase of oxygen binding energy which boosts the initial dehydrogenation rate [62].

Platinum–rhenium

Pt–Re/C was initially studied for the gas-phase glycerol reforming, where it was noted that the H_2 turn over frequency (TOF) increased by one order of magnitude compared to Pt/C [63]. In a simplified kinetic model, the authors observed that the CO adsorption equilibrium constant was 10 times lower for the bimetallic catalyst compared with the monometallic. Kunkes et al. carried out microcalorimetric measurements of CO adsorption and CO-TPD studies [64]. Pt/C catalyst reported 115 kJ/mol as heat of CO adsorption, while for Pt–Re/C catalyst it approached the one of pure Re (105 kJ/mol). Moreover, the partial oxidation of Re sites under the APR condition may form sites with lower binding energies. Avoiding that the sites are blocked by CO (or other intermediates) is of paramount importance because C–C bond breaking mainly happens with transition states multiply bonded to Pt sites, therefore the latter must be preferably free [21]. Thanks to attenuated total reflection-infrared (ATR-IR) in situ analysis, it was reported that CO desorption from catalyst surface was more facile on the bimetallic catalyst compared to the monometallic [65]. ReO_x can interact with CO adsorbed on Pt, facilitating its desorption (CO spillover), contributing in this way to the increase of activity. Another reason for the higher activity can be related to the increased C–C and C–O bond breaking capacity, with the latter to a major extent. It means that the Re addition decreased the hydrogen selectivity because it favored hydrogenation reactions of dehydrated intermediates. This is because Re increased the acidity (Re-OH, Brønsted type) of the catalytic system.

King et al. tested Pt–Re for the first time under APR conditions [66]. Re addition led to an increase of glycerol and H_2 TOF. Re alone did not show any activity, so the effect was just as promoter. However, it decreased the H_2 selectivity. As previously reported, the promotion was induced by multiple reasons: on one side, Pt–Re alloy can have higher activity by modification of the electronic properties that can affect the CO adsorption strength. Moreover, Re can favor water gas shift by water activation, which is limited on platinum [67]; in this way, higher OH surface coverage may be obtained, leading to a higher formation of COOH, which is a key intermediate for the reaction. This outcome was proved by CO stripping voltammetry in Ref. [68], where the authors observed that the Pt–Re had a lower onset potential of CO oxidation than Pt one, and it was ascribed to a higher concentration of OH species (stronger binding of oxygen species which promoted water activation). Finally, the acidic properties could explain the decrease in H_2 selectivity. KOH addition showed further increase in liquid products, so that it can be assumed that base addition can compensate the surface acidity provided by ReOH.

The correlation between the surface properties of the bimetallic catalyst and the product distribution was further investigated in Ref. [69]. XPS showed that Pt binding energy (BE) shifted, and it was higher with higher Re loading. The increase of the BE (electron deficiency) was due to the interaction with Re (possibly alloy formation). However, Re BE increased as well, ascribed to metal-support interaction. In order to simulate the interaction with water, the catalyst was

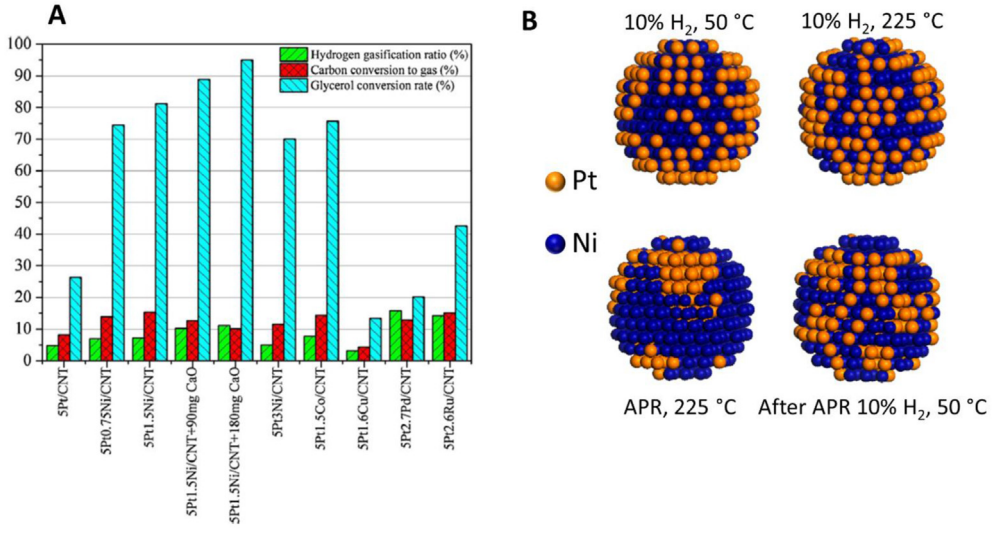

Fig. 11 – A: Effect of promoters and additives on the APR of glycerol, reaction conditions: 230 °C/30 bar initial N_2, 10 wt% glycerol solution, 0.1 g catalyst, 4 h (from Ref. [59]). The y-axis refers, with the same units of measure, to hydrogen gasification ratio (green bars), carbon conversion to gas (red bars) and glycerol conversion rate (light blue bars); B: Structure of the Pt–Ni particles at reduced conditions, during APR and after regeneration (Reprinted with permission from Ref. [61]. Copyright 2012 American Chemical Society). (For interpretation of the references to color in this figure legend, the reader is referred to the Web version of this article.)

treated with steam, leading to a change of oxidation in both platinum and rhenium. In particular, the presence of new Re-OH species increased the surface acidity, which in turn affected the product distribution favoring dehydration products via acid-catalyzed reactions. Interestingly, it was reported that the hydrogen selectivity increased with the conversion: this is due to the more difficult dehydration of smaller molecules compared with glycerol. Similar conclusions were reported in Ref. [70] and in the case of xylitol [71].

In conclusion, it is worthy to highlight some of the outcome reported for these characteristic bimetallic Pt-based catalysts. Table 1 resumes the effects of Mo, Co, Ni and Re addition to Pt, as reported in the last sub-paragraphs. Commonly the promoters induced an electronic perturbation of platinum, which decreased the interaction with the adsorbates and increased the availability of free active sites. Apart from Co, each of the promoters caused a strong increase of the conversion but associated with a decrease of the H_2 selectivity. In fact, often the C–O cleavage pathway is favored: for example, due to the enrichment of surface acidity in the case of Re, or due to methanation in the case of Ni. It is important to observe that tuning the reaction conditions, like adding a base, could overcome the reported drawbacks.

Ni-based catalysts

In view of a possible industrial application of APR, the use of non-noble metals in the catalyst formulation may be a milestone for the success. For this reason, the use of transition metals-based catalysts, such as Ni, has been explored.

Rahman investigated bimetallic Ni-based catalysts for APR of glycerol over multiwalled carbon nanotubes [72]. In the 1 Pt-xNi series, 1 Pt–3Ni was found the one with the highest activity (glycerol conversion higher than 99%) and hydrogen yield (Fig. 12-A). Monometallic Ni was confirmed active towards methanation, reporting the highest yield for methane and the lowest glycerol conversion (44%). As depicted in Fig. 12-B, Ni influenced the electronic state of Pt (shift of the binding energy). While Ni monometallic suffered from deactivation after 65 h TOS, Cu and Pt addition allowed to maintain a stable hydrogen production in 100 h long runs.

The influence of several promoters (Mg, Cu, Zn, Sn, Mn) on the APR of ethylene glycol was recently studied over Ni–Al hydrotalcites [73]. The screening reported that the conversion was not affected by the incorporated metal. On the other hand, the selectivity was improved in the case of Mg promoter. The authors explained this outcome because of the change in the electronegativity of Ni. Interacting with MgAlO, Ni became more electronegative, reducing the possibility that the feed may be dehydrated.

Luo et al. studied the Ni:Co ratio for APR of glycerol on alumina support [74]. 1:3 was found the optimal ratio to maximize the hydrogen yield, thanks to the tradeoff between higher selectivity thanks to Co addition and lower activity due to the decrease of superficial Ni. The synergy between the two metals, proved by H_2-TPR, was confirmed by the fact that both monometallics had much lower hydrogen yield. Slight addition of Ce further increased the hydrogen yield promoting the formation of NiO instead of Ni aluminate, improving the dispersion, and decreasing methane selectivity. Moreover, it avoided Ni sintering and stabilized the alumina support. Nevertheless, coke remained one of the causes for catalyst deactivation.

The effect of cobalt addition to a bimetallic Ni–Fe catalyst was systematically studied thanks to Fourier-transform infrared spectroscopy (FTIR) characterization before and after APR of ethylene glycol [75]. The results are reported in Fig. 13. Ni was found to be responsible for ethylene glycol activation (about 30% carbon conversion to gas for Ni alone vs 10% for Fe alone) thanks to the high activity of metallic Ni for C–C bond breaking. The bimetallic Ni–Fe further improved the conversion at 45%, also reaching higher hydrogen selectivity. Fe was present as Fe_3O_4 and was supposed to be involved in the WGS via a redox mechanism: Fe^{2+} was oxidized by water (producing hydrogen) to Fe^{3+}; afterwards, the latter was reduced back by CO (producing carbon dioxide). The addition of Co strongly increased the conversion up to 95%, maintaining the hydrogen selectivity but at the same time cutting the alkane selectivity from 75% to less than 5%. It was suggested that Co increased the capacity to adsorb ethylene glycol at the same time decreasing the one for hydrogen. Finally, the authors highlighted the instability of the catalyst due to the re-oxidation of Fe and leaching of Ni.

Further improvements of Ni catalyst were reported in Ref. [76]. A Ni–B amorphous alloy catalyst showed higher hydrogen production and stability than Raney Ni: the improvement was attributed to the boron oxides which, surrounding the hexagonal close-packed Ni, caused their stabilization and the higher resistance against sintering.

Nickel–copper

Tuza et al. studied Ni–Cu catalysts supported on hydrotalcite-like compounds, with varying composition from 20% Ni monometallic to 20% Ni–20% Cu [77]. Ni monometallic showed the highest activity among the samples. The addition of copper increased the Ni dispersion and reducibility. The increase of hydrogen selectivity (250 °C) during 12 h TOS was ascribed to the lower particle size, since multiple Ni clusters are necessary for CO dissociation and methane production. At 270 °C a decrease of the hydrogen selectivity (defined by the authors as the molar fraction in the gas phase) with TOS was observed because of hydrogen-consuming reactions (acetol hydrogenation), with increase of CO_2 selectivity.

In a successive work, Manfro et al. looked also at surface acidity properties [78]. They observed that bimetallic catalysts were more acidic than monometallic, explaining the higher acetol formation. The absence of re-oxidation contrarily to other case reported in literature was motivated by the stabilization of the support. The slight sintering that occurred did not cause deactivation in 6 h TOS.

Ni–Cu supported on MWCNT for glycerol APR was also run up to 110 h, in order to get information also on extended time on stream [79]. X-ray diffraction (XRD) spectra showed a shift in the Ni peak, indicating the higher interaction with Cu in the case of higher loading, with possibility of an alloy due to their complete miscibility. Moreover, the dispersion increased when Cu was added (further increase led to similar dispersion than the monometallic). At the same way, the 1Cu12Ni was the most stable against sintering. The catalytic tests showed superior performance of the bimetallic formulation, with 1Cu12Ni giving

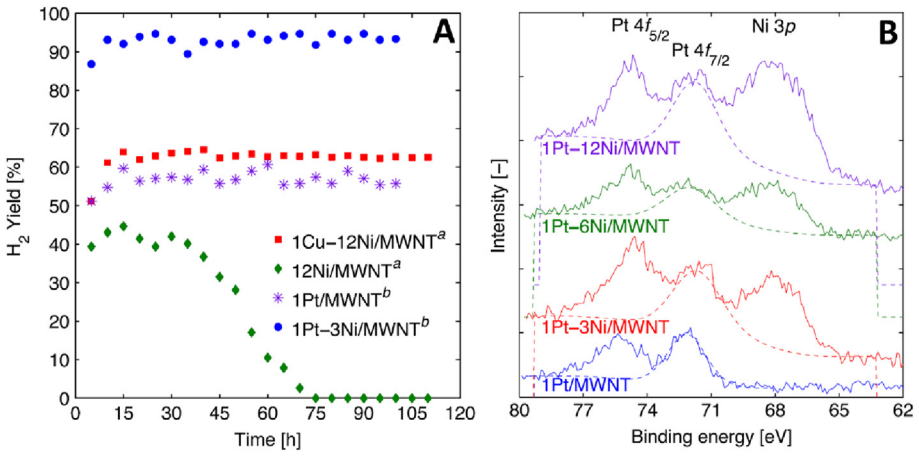

Fig. 12 – A: Hydrogen yield obtained from APR of glycerol, reaction conditions: 240 °C/40 bar, 1 wt% glycerol, 0.05 mL/min, 0.1/0.15 g of catalyst (a and b respectively, in the legend); B: XPS patterns of reduced catalysts (from Ref. [72]).

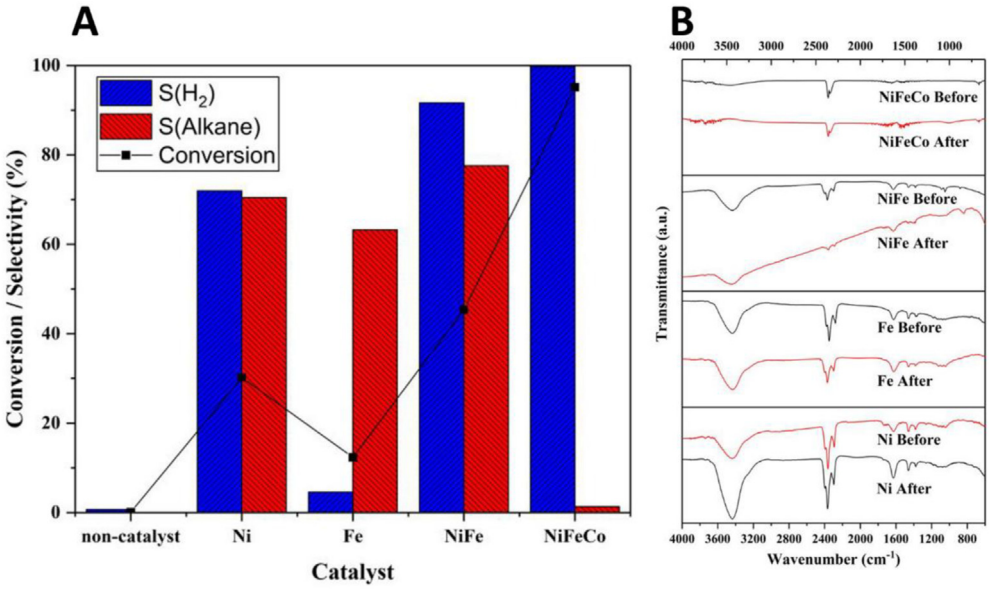

Fig. 13 – A: Catalytic performance of different catalysts for APR of ethylene glycol, reaction conditions: 225 °C/26 bar, 20 wt% ethylene glycol, 0.2 g catalyst; B: FTIR patterns before and after the reaction (Reprinted with permission from Ref. [75]. Copyright 2020 American Chemical Society).

the highest hydrogen yield. It reported lower CO ascribed to the higher WGS activity; moreover, methanation activity of Ni decreased, attributed to the alloy formation and the reduction number of clusters with multiple Ni atoms which are necessary for CO hydrogenation (4-fold lower methane formation in the bimetallic catalyst compared to the monometallic one). Looking at the stability, 6Cu12Ni and 12Cu12Ni showed high sintering, while 1Cu12Ni did not, leading stable H_2 yield along three consecutive 110 h TOS runs. Only minor sintering was observed, but no re-oxidation for Cu and Ni and leaching. WGS activity was assessed with a proper test.

Park et al. studied different Ni-based catalysts supported on $LaAlO_3$ with different promoters (Cu, Co, Fe) and found that Ni–Cu was the one with highest glycerol conversion and hydrogen selectivity [80]. It was the catalyst with the highest dispersion, while the monometallic Ni showed the worst dispersion. Furthermore, it showed less coke deposition (whisker type, less harmful because it grows on one side of the metal particle) than the monometallic (graphite type) and no sintering (contrarily to the monometallic). However, it was higher than the Ni–Co formulation.

Table 2 summarizes the effects of the promoters on the performance of APR when added to Ni-based catalysts. Since the beginning of the APR research, Ni has been reported as one of the most interesting non-noble metals due to its high activity. The addition of the promoters like Sn, Mg, Co and Cu helped to increase the selectivity by different mechanisms (e.g. by blocking defect sites or decreasing the particle size). This outcome is a key improvement since the lack of selectivity due to the high tendency of methanation is a drawback

Table 2 – Influence of the promoters on Ni-based catalysts for APR reaction.

Catalytic system	Modification caused by the promoter	Drawbacks/unsolved issues	Reference
Ni–Sn	Suppression of CO methanation by Sn decoration of Ni-defect sites; higher resistance to Ni sintering	TOF for hydrogen production more than three times lower than conventional Pt-based catalysts	[32,33]
Ni–Mg	Higher H_2 selectivity thanks to the increase of Ni electronegativity, reducing the dehydration pathway		[73]
Ni–Co	Higher H_2 selectivity	Lower C–C activity Carbon deposition and sintering	[74]
	Higher conversion thanks to higher substrate adsorption and lower H_2 adsorption	Leaching	[75]
Ni–Ce	Higher activity thanks to improved dispersion	Carbon deposition	[74]
Ni–Fe	Higher substrate conversion thanks to WGS promotion	Re-oxidation	[75]
Ni–B	Higher sintering resistance		[76]
Ni–Cu	Higher H_2 selectivity thanks to higher dispersion	Lower H_2 selectivity at high temperature	[77]
	Higher H_2 yield thanks to higher Ni dispersion and reducibility	Dehydration promotion due to higher acidity	[78]
	Higher H_2 yield thanks to WGS promotion and reduction methanation activity; no re-oxidation		[79]
	Higher H_2 yield thanks to WGS promotion and higher dispersion; no sintering and graphite-type coke	Whisker-type coke deposition	[80]

of Ni-based catalysts. At the same way, most of the unsolved issues still regards the instability by re-oxidation, carbon deposition or leaching, which may prevent a long-term use.

Other catalysts

Apart from the catalytic systems previously reported, some others are worthy to be cited. In fact, despite they may be less frequently applied, their outcome may be interesting to stimulate further research. Therefore, in the following, formulations based on noble metals (Ir and Ru), bulk and metal-free catalysts will be reported.

Liu et al. tailored the properties of a Ir-ReO_x/SiO_2 catalyst with a noble metal (Ru, Pd, Pt) to favor either the APR of glycerol (C–C breaking) or its hydrogenolysis (C–O breaking) [81]. Pt showed higher conversion compared to Ru and Pd, but lower selectivity to acetol and propylene glycol (1,2-PrD), due to its higher selectivity towards APR. Being the particle size similar, it cannot be ascribed to structure-sensitivity features. Increasing the conversion led to an increase in the C3 products selectivity. This is coherent with previous literature since hydrogen selectivity decreased with the reaction time due to parasite consecutive hydrogenation reactions. The properties of the Pt–Ir-Re system were investigated looking at the monometallic and combination of bimetallic (Fig. 14). Ir provided the highest conversion among the monometallic and the highest selectivity to acetol. Pt–Ir and Ir–Re showed higher conversion than the monometallic, with the former providing more APR activity: this is suggested by the higher presence of hydrogen and propylene glycol, meaning that more hydrogen was produced. This outcome showed the synergy among Pt and Ir since the corresponding monometallic catalysts reported very low activity. The authors suggested that new species were formed, with XRD showing a shift in the Pt and Ir peaks indicating the formation of alloys. The physically mixed catalyst had similar conversion level to the Ir-ReO_x/SiO_2 but lower than the trimetallic, underlying the importance of the proximity between the components, which cannot be obtained through a simple mixing. Adding ReO_x allowed to reduce the metal particle size. Finally, it was observed that low loading of Pt (and likely smaller particles) favored the C–O hydrogenolysis.

Espinosa-Moreno et al. studied the APR of glycerol over Ir-based bimetallic catalysts with Cu and Ni [82]. The authors observed that Ir–Cu led only to 0.9% of carbon conversion to gas, despite the high glycerol conversion (76.5% on La_2O_3 support). This result was not trivial from literature. In fact, Ir was initially suggested by Dumesic and coworkers as a plausible APR catalyst thanks to its high hydrogenolysis activity (referring to the work of Sinfelt [83]). The addition of Cu was not sufficient to overcome the WGS limitation and the possibility that CO poisoned it.

The performance of Ru-based catalyst was improved as well thanks to the use of promoters, under multiple points of view. Its stability was improved thanks to the use of nitrogen, which avoided Ru sintering increasing the metal-support interaction, favoring at the same time the initial dispersion [84]. At the same time, higher glycerol conversion and hydrogen selectivity were obtained. Moreover, it exalted the basicity of the support. This feature helped to activate the water molecule, which is a necessary step for the WGS reaction: its facilitation allowed to improve the overall performance because the sites were less occupied by the CO.

Novel unconventional types of catalysts can be finally reported, such as the use of cobalt aluminate spinel for the APR of glycerol [85] and metal-free catalysts [86]. Cobalt is not

stable due to oxidation and leaching. However, the spinel formation with alumina may overcome these limitations. Thanks to a mutual protective effect, the spinel catalysts had surface area higher than cobalt oxide and alumina alone. Increasing the Co loading decreased the surface acidity (measured by NH_3-TPD) because alumina, which is a Lewis acid, was substituted by cobalt oxide. Analogously, basic sites formation was favored by Co loading (measured by CO_2-TPD). Reference tests with alumina and cobalt oxide alone gave respectively the highest and lowest selectivity for hydroxyacetone, which is acid-catalyzed; at the same time Co_3O_4 gave the highest H_2 and CH_4 selectivity, being methanation favored by basic sites. The spinel structure helped in reducing the methanation activity and the re-oxidation of Co (5% vs 10%), even in a reducing atmosphere. The results showed the predominance of C3 liquid products, highlighting the low activity for C–C breaking of Co. The conversion decreased with time on stream also due to coke and sintering of large particles.

Esteve-Adell et al. used for the first time a metal-free catalyst to perform the APR of ethylene glycol, i.e. graphene, obtained by alginate pyrolysis [86]. In this context, the presence of defects is pivotal to activate reactions that commonly require metals to overcome kinetic limitations. Graphene allowed higher conversion compared to graphite-derived materials. One main point of concern was the low stability, that ended up in negligible activity at the third run. It was ascribed to the possibility that carboxylic acids by-products or hydrogen itself may react with the active sites (carbonyl groups and diketones). In particular, the author proposed that they consist of frustrated acid-base Lewis pairs, i.e., Lewis acid and bases close enough to interact with H_2 but not enough to interact between each other, acting as dehydrogenation sites. IR spectra and thermogravimetric analysis showed the presence of adsorbate organics.

Influence of particle size

Before moving on the third element chosen by the catalyst designer, the choice of the support, it is worthy to discuss one issue still related to the active metal category. It has been proven that aqueous phase reforming is a structure-sensitive reaction, i.e., its rate, normalized per exposed metal surface atom, changes with the particle size [87]. However, in the APR field, there is no apparent agreement if smaller of bigger particles are more benefic for hydrogen production. In the following, the main works analyzing this topic are reported. Despite in some cases TOF was not reported, valuable comments can be drawn.

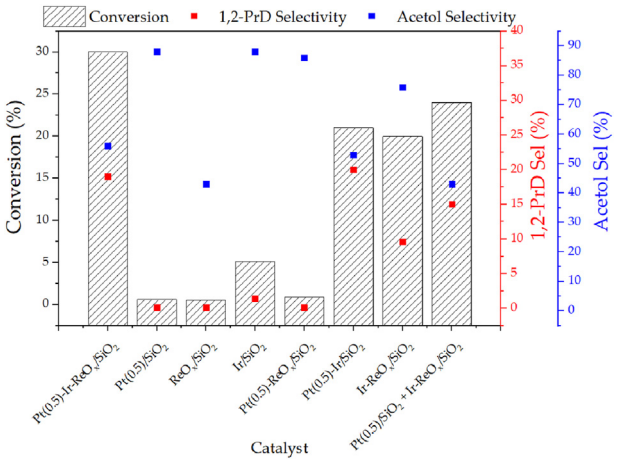

Fig. 14 – APR of glycerol over different Pt and/Ir supported catalysts. Reaction conditions: 190 °C/20 bar Ar, 10 wt% glycerol, 17 h (data from Ref. [81]).

Lehnert and Claus reported for the first time that hydrogen selectivity increased with increasing particle size, without affecting the conversion (Fig. 15-A) [88]. Increasing the particle size implies that the number of face atoms increases, while the number of edges and corner atoms decreases [89]. Therefore, it can be postulated that a greater extent of face atoms permits favorable adsorption of the oxygenates for the C–C breaking.

On the other hand, Wawrzetz et al. reported different results. Despite the agreement on the fact that the conversion was slightly affected by the particle size, they reported higher hydrogen selectivity for smaller particles (Fig. 15-B) [90]. This result was ascribed to the higher concentration of metal sites that hindered the dehydration pathway (i.e., the catalytic chemistry favored by the support). Having smaller particles means highly coordinatively unsaturated metal atoms and at the same time higher concentration of metal atoms at the support-metal boundary. Both aspects may affect the mechanism followed by the molecule and its fate (hydrogen or alkane production).

The latter outcome was supported by the results reported in Ref. [91], where small Pt particles favored C–C breaking more than C–O. Moreover, sintering happened during the first 60 min (from approximately 2 nm to less than 4 nm) and then it was constant up to 1440 min. Similar results were reported for Pt particles in Refs. [92–94], where quantum effects have been proposed to explain the change of TOF close to a critical diameter. Moreover, methanation is favored by bigger particles [36].

Very recently, Vikla et al. prepared different Pt/Sibunit catalysts not only to study Pt size effects, but also looking at the influence of its distribution (uniform or egg-shell) [95]. The hydrogen production rate, normalized per unit of surface Pt, linearly increased with the mean particle size (up to 10.7 nm), in accordance with [88]. Furthermore, an optimal size for the agglomerated particles was found (about 21 nm).

A change in the activity was reported in Ref. [96], where platinum nanoparticles with different particle size were synthesized for glycerol APR to obtain structure-activity relationship. Normalizing to the Pt surface area, it was showed that larger particles increased the conversion (the activity). Moreover, the product distribution was affected (the selectivity). It was reported that small particles (with higher concentration of edge sites – Pt(100)) favored the dehydrogenation, while larger particles (with higher concentration of facet sites – Pt(111)) favored the dehydration.

A stability-related TOF was defined by Duarte et al., who looked at the influence of Pt loading on alumina supported catalysts (0.3–2.77 wt%) by IWI [97]. The authors reported that the amount of coke decreased when the number of surface Pt increased; in other words, larger particles caused less coke

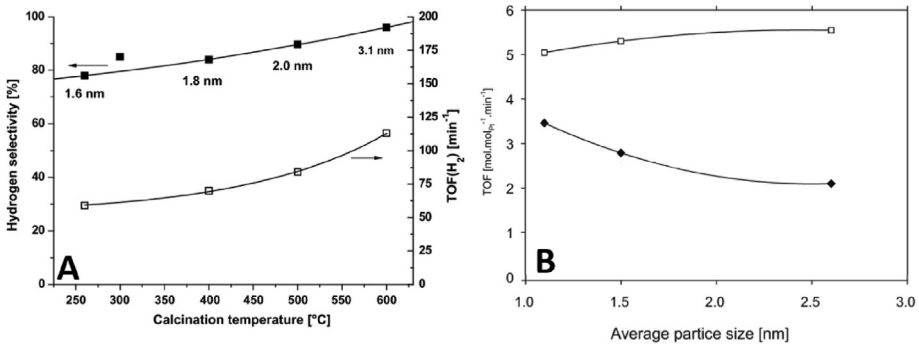

Fig. 15 – A: Influence of particle size on APR performance. Reaction conditions: 250 °C/20 bar Argon, 10 wt% glycerol solution, 0.5 mL/min, 0.3 g 3% Pt/Al_2O_3 (Puralox) (from Ref. [88]). Blank squares TOF for hydrogen production, full squares TOF for hydrogen selectivity; B: Reaction conditions: 225 °C/29 bar, 20 wt% glycerol solution (modified from Ref. [90]). Blank squares TOF for glycerol conversion, full squares TOF for hydrogen production.

deposition. Moreover, sintering was observed for all the catalysts, and that was proved to occur during the initial phase of the reaction, since no decay in the performance was observed. The same research group previously studied the effect of Pt loading on xylitol APR in Ref. [98] and sorbitol [99].

Higher H_2 TOF for smaller particles were observed also for Ru-based catalysts [100]. The use of in-situ ATR allowed the authors to observe that on the catalyst with high loading (5 wt %) and large particles (4 nm) C–O breaking bond was favored, leading to acetylide intermediates and methane as the final product. On the other hand, the catalyst with low loading (0.5 wt%) and small particles (1 nm) did not lead to any acetylide. The difference was attributed to the fact that acetylide needs two bonds with the metallic site, therefore it was more likely to happen on flat metallic surface. Analogous outcome can be found in Ref. [101], where Ru catalysts were prepared at different loading to have particle size greater than 2 nm (representatives of high-coordination flat terraces) and smaller than 2 nm (representatives of low coordination step/edges). They observed that small Ru particles favored hydrogen selectivity, with CH_4/H_2 ratio less than one. At the same time, the C1/C2 products ratio is smaller, indicating less activity for breaking. This result is contrast with DFT studies, which foresee lower energy barriers on smaller particles rich in edges and steps. The discrepancy was ascribed to the possibility that more active smaller sites can be deactivated by CO blocking which is strongly adsorbed. To confirm this hypothesis, Fischer-Tropsch synthesis was carried out, which did not report alkane formation on small Ru particles because CO was not activated.

Van Haasterecht et al. studied the influence of Ni particle size on different supports (carbon nanofibers, alfa and gamma alumina, zirconia, SiC) for APR of ethylene glycol [102]. Narrower peaks in the XRD of spent catalysts, together with TEM images, confirmed that sintering phenomena occurred for each of the supported catalyst in this order: CNF > ZrO_2 > SiC > γ-Al_2O_3 > α-Al_2O_3. The difference was attributed to the different inter-particle distance (due to the different surface area) and the initial particle size. The authors reported that smaller particles grow faster and more than bigger particles; furthermore, they suggested that it was due to Ostwald ripening mechanism due to the high solubility of Ni and absence of the influence of the catalyst loading on the growth rate.

Effect of supports

In heterogeneous catalysis the function of the support is typically reported as a mean to increase the metal dispersion. However, its behavior may be active in determining the performance of the reaction. For example, the acid-base functionalities of the supports are well-known and exploited in many important industrial reactions, such as hydroisomerization. In the context of APR, the nature of the support has been reported as a mean for tuning the hydrogen production.

The support can affect the quality of the hydrogenation sites [103] due to its electronegativity. In the case of APR, it has been reported that Pt/alumina is less hydrogenating because of the lower electronegativity of the support compared to Pt/amorphous silica alumina [104].

Shabaker et al. screened different supports for platinum-based catalysts [105]. Looking at the H_2 TOF reported in Fig. 16, the ranking at 225 °C was TiO_2 > black, carbon, Al_2O_3 > SiO_2–Al_2O_3, ZrO_2 > CeO_2, ZnO, SiO_2, with Al_2O_3, ZrO_2 and TiO_2 showing the highest hydrogen selectivity. The reaction temperature significantly influenced the ranking, with Pt-black being the one with the second worst TOF at 210 °C. SiO_2 and CeO_2 were reported to dissolve under the hydrothermal conditions.

As reported in the introduction, the support has a strong role in modifying the hydrogen selectivity because of its acid-base properties. Wen et al. studied the effect of supports with different acidity with a Pt-based catalyst [106]. The authors showed that the scale of hydrogen yield was SAPO-11 < AC < HUSY < SiO_2 < MgO < Al_2O_3, which is qualitatively coherent with the range of acidity (i.e., SAPO-11 and HUSY are zeolites, while MgO is a basic support). During 240 min TOS, each support was stable except for MgO and SAPO-11. Possible structure-sensitivity effects were excluded in Ref. [38] by pre-synthesizing platinum colloids that were

then loaded on the supports through different techniques. It was pointed out that the scale of basicity (measured via CO_2-TPD) was analogous to the range of hydrogen yield, i.e., $MgO > Al_2O_3 > CeO_2 > TiO_2 > SiO_2$. The authors suggested that the support basicity polarized water, inducing its dissociation and facilitating the WGS step. Again, although MgO showed the best performance, it was not hydrothermally stable. Further screening of supports highlighted the importance of the basicity for Pt-based catalysts in Ref. [107].

Liu et al. studied different supports for Pd-based catalysts in the APR of ethylene glycol [108]. Among NiO, Cr_2O_3, Al_2O_3, ZrO_2, Fe_2O_3 and Fe_3O_4, the latter showed the best performance thanks to the promotion of the water gas shift, which is the rate determining step for Pd.

Kim et al. investigated the effect of support on Pt–Re systems [109]. The authors reported that the activity increased in the order alumina < silica < activated carbon < CMK-3. The ordered mesoporous carbon was explained as the best thanks to the easier access of the active site for the reactants and escape of the products and higher dispersion. Similar outcome was obtained by CMK-9 in the case of Pt-Fe [41].

Zirconia and boehmite supports were explored in the APR of hydroxyacetone [110]. The support alone (and zirconia notably) produced more coke than the platinum-supported catalyst (measured by CHN analysis and temperature programmed oxidation), indicating that the metal plays a role in preventing such deactivation via aldol condensation mechanism. Boehmite may have fewer coke thanks to its lower acidity. The in-situ ATR study allowed identifying the most present dimer between the two possible intermediates.

It is interesting to observe also the influence that the support modification may have on the stability of the entire catalytic system. Stekrova et al. studied the influence of different Ce, Zr and La oxide supports for the APR of methanol [111]. Nickel catalysts are often subjected to deactivation due to re-

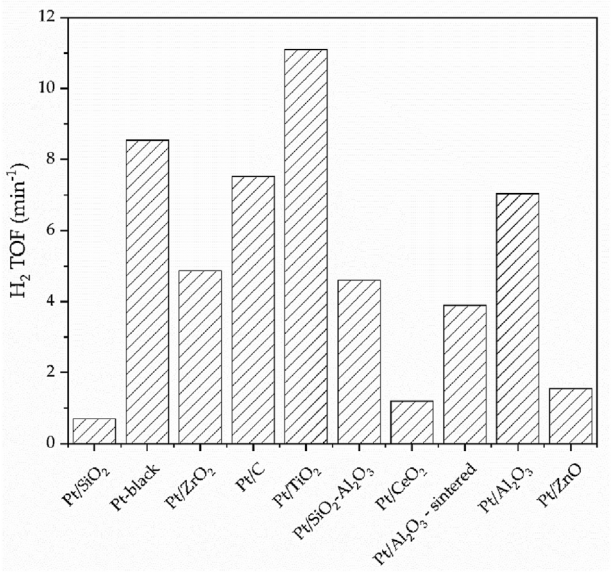

Fig. 16 – Influence of the support on APR of ethylene glycol. Reaction conditions: 225 °C, 10 wt % ethylene glycol solution (data from Ref. [105]).

oxidation and sintering of the metal particles. ZrO_2 and CeO_2 thanks to their oxygen storage and mobility are useful supports for WGS. Furthermore, oxygen vacancies can be increased if doped with lower-valence metal, like La, also increasing the metal-support interaction and, consequently, the Ni dispersion. The authors showed that Ni did not re-oxidize during the reaction. However, atomic absorption spectroscopy showed the occurring of Ni leaching. Ni sintering also occurred during the reduction step. While it was the same for pure zirconia and mixed ceria-zirconia oxide, it was lower in the case of mixed Ce–La, likely due to the strong interaction between Ni and La. Cerium carbonate was reported as the main cause for the deactivation of the WGS step, even if the activity was restored by thermal regeneration (300 °C, air flow). Looking at the performance of APR, they reported that the use of mixed oxides is beneficial for the activity. Surprisingly, pure CeO_2 support showed the lowest WGS activity, despite its effectiveness in the gas-phase system. On the other hand, the highest WGS activity was reported by mixed 17Ce–5La–Zr support, linked to its highest basicity.

Table 3 summarizes the main effects of the support on the performance of APR. The acid -base properties and the reducibility were mostly investigated since they are directly involved in the water gas shift step that, as reported throughout this work, is a key step to promote the hydrogen yield. Less attention has been put on the textural properties, despite it can be important to promote the selectivity. In fact, it can be favored not only playing with the nature of the active sites, but also avoiding that hydrogen, once produced, may contact other feed molecules/intermediated and hydrogenate them.

Alumina

Alumina is one of the most studied supports for APR. Different alumina supports for Pt catalysts were studied in the APR of ethylene glycol [113]. It was reported that the hydrogen yield decreased in the order alfa > delta > gamma thanks to the high dispersion obtained in the former. The authors reported that the absence of chlorine in the alfa sample (prepared with a higher temperature treatment compared with gamma) improved the dispersion because chloride facilitated the sintering. Moreover, it was suggested that Pt is more anchored on dry (e.g. alfa) alumina surface than on the hydroxylated one (gamma).

Making an analogy with the active site, it has been reported that binary supports, i.e., mixed oxides, are able to increase the hydrogen production thanks to a synergy between the components. α-Al_2O_3 modified with CeO_2 and ZrO_2 improved by more than 50% the hydrogen yield compared to unmodified α-Al_2O_3 [91]. This is because CeO_2 and ZrO_2 participate in the water activation, therefore promoting the WGS reaction [114].

Iriondo et al. modified alumina-supported Ni-based catalysts with Mg, Ce, Zr or La for glycerol APR [115]. La addition caused the highest increase in glycerol conversion, followed by Ce, Zr and Mg which was worse than the un-modified alumina. The supports did not influence the selectivity. Neither affected the dispersion, as there was not a clear trend. The authors suggested that geometric effects were due to the presence of the promoters on the Ni surface, similarly to Sn on

Ni. All the samples showed deactivation ascribed to re-oxidation of Ni, while sintering was not reported.

The influence of two different supports (alumina and nickel aluminate) have been studied for the aqueous phase reforming of methanol [112]. Pt supported on $NiAl_2O_4$ showed higher dispersion than on alumina (80% vs. 70%). The use of the spinel increased the methanol conversion from 26.5% to 99.9% and the hydrogen yield from 23.3% to 95.7%. Please note that in this case, Ni was present in an oxide state, so it was not able to activate the methanation reaction. Being $NiAl_2O_4$ not able to convert methanol, a synergy between the active site and the support was supposed to explain the improvement of the performance, due to several reasons. In situ DRIFTS was used to detail the CO formation process for the first time, showing that it is achieved via dehydrogenation of methanol to methoxy and formaldehyde species, followed by the decomposition of the latter to CO. Interestingly, the pathway was different for the alumina-supported catalyst. Indeed, it had mediocre dehydrogenation activity (the formation of formaldehyde and CO was observed at a longer time) and WGS (peaks of CO were already present, while they were absent for the spinel-supported catalyst). In the spinel support, platinum was more reducible, therefore more active for dehydrogenation (first reason for the synergy); the motivation was ascribed to the oxygen vacancy present in $NiAl_2O_4$. Furthermore, they contributed to carry out the water gas shift activating water via a redox mechanism which is faster than the associative mechanism observed for alumina. Summarizing, as reported in Fig. 17, the first step (dehydrogenation) is performed in the same way on both catalysts: playing Pt a vital role for dehydrogenation, its characteristics affected the performance, and they improved thanks to the fact that it was more reducible. In the second step, the efficacy of WGS was further prompted by the redox mechanism, rather than the associative one.

Moreover, the catalyst was stable along 600 h of time on stream, with only 10% of loss in conversion (no information on the possible change of selectivity were reported).

Ceria support showed higher dispersion, WGS activity and resistance to coke than alumina [116]. Furthermore it suppressed methanation [117] by poisoning the responsible active sites. This mechanism would be analogous with the one proposed for the Sn-modified Ni Raney [32]. The effect of CeO_2 addition to alumina supports for Pt catalysts in APR of glycerol was studied for the first time in Ref. [118]. 3% and 6% ceria doping increased the hydrogen and methane yield compared to unpromoted alumina, while 9% loading decreased the hydrogen yield. The catalysts showed similar hydrogen selectivity. The authors ascribed the improvements to the increase in the availability of metal surface area and reducibility of platinum precursor by adding ceria.

Bastan et al. looked at the APR of glycerol over Ni-based catalyst supported on mixed alumina/MgO oxide, searching for a structure-activity relationship for the different Al/Mg ratio [119]. As reported previously, Ni suffers from sintering. MgO can be used to stabilize Ni particles. Increasing the Mg content also increased the Ni dispersion, while decreasing its reducibility. The A2M1 support showed the highest conversion because of the higher presence of surface metallic Ni. The spent catalyst showed re-oxidation of Ni and no carbon deposition, while no information on sintering was reported. Despite of the re-oxidation, the study of the performance showed stable hydrogen yield along 24 h of time on stream.

$Pt/SiO_2–Al_2O_3$ with different Si/Al molar ratio (range 0–1) was investigated to modify the surface acidity and influence the product distribution [120]. Maximum conversion and hydrogen production rate were reported at Si/Al ratio equals to 0.1. Increasing the ratio led to an increase of the methane selectivity and a decrease of ethane selectivity. The authors reported that increasing the Si loading led to an increase of the Brønsted/Lewis acidity ratio (because Si–OH species are present on the surface), as well as an increase of the weak acidic sites and a decrease of the strong (and total) acidic sites. This difference on the quality and quantity of acidic sites can alter the platinum dispersion as well (higher at higher Si/Al ratio). The authors correlated the conversion with the amount of strong acid sites and the hydrocarbon selectivity to the weak Brønsted acid sites. However, contrarily to most of the works reported in literature, the authors assumed that higher alkane selectivity can be attributed to both C–O and C–C cleavage.

Despite the promising use of alumina, its transition into boehmite is well known under APR conditions, as reported in Refs. [121,122]. The use of silica deposition has been explored to overcome this limitation [123]. During the structural modification into boehmite, the metal particles may be encapsulated or sinter due to the losing contact with the support. One strategy to prevent this occurrence is increasing the support hydrophobicity, preventing the Al centers attack. The authors used tetraethylorthosilicate (TEOS). The total acidity decreased (measured by NH_3-TPD), due to the substantial decrease of Lewis acidity (measured by pyridine adsorption) and a small increase of Brønsted acid sites. The silylation decreased the catalyst activity: the complete conversion was reached for pure alumina after 5 h, while the necessary time increased up to 7 h and 12 h with the increase of silylation time (0, 4, 8, 12 h). In Fig. 18-A the modification of the hydrogen production rate is reported. The rise in acidity

Table 3 – Influence of the support on the APR performance.

Property of the Support	Main effect	Example	Reference
Acid-Base	Higher H_2 yield since support basicity polarizes water, promoting the WGS	MgO	[38,106,107]
	Higher coke formation in the presence of higher acidity	ZrO_2	[110]
Redox couple	WGS promotion by redox mechanism	Fe_3O_4, $NiAl_2O_4$	[108,112]
Mesoporosity	Easy transport of reagents and products into the catalyst	CMK-3	[41,109]
Oxygen storage and mobility	WGS promotion	CeO_2	[111]

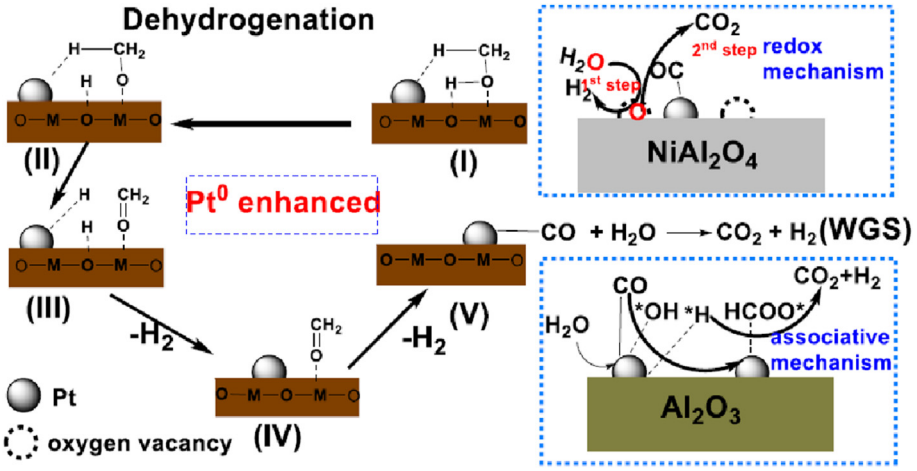

Fig. 17 – APR reaction mechanism reported for methanol on different supports (from Ref. [112]).

caused the increase in hydroxyacetone selectivity; the WGS remained effective (lack of CO). The boehmite formation was slowed down or prevented, while some minor sintering occurred. Globally, the support life-time increased from 12 h to 36 h, likely due to the removal of the protective layer.

Similarly, Van Cleve et al. used alkyl phosphonate coatings to improve alumina hydrothermal stability [124]. The authors investigated phosphonic acids with different tail lengths, from C1 to C18. The initial surface area decreased due to this pretreatment likely because of the blockage of smaller pores. While alumina became boehmite if untreated, the alkyl phosphonate slowed down the transition, and it was slower the longer the tail length (Fig. 18-B). The reason may be ascribed to the hydrophobic properties or the density (the smaller the chain, the higher the loading) of phosphonate groups. The role of the tails was investigated after an oxidative treatment where the tails were removed. Since alumina remained stable, it was suggested that the key to the improvement was the interaction between the support and the head of the alkyl phosphonate. Nevertheless, the longer chain (C18) showed higher stability despite the lower P density. It may be since the high coverage of C1 led, on average, to lower coordination compared to C18, so that the support was less stabilized.

Zirconia

The addition of cerium, yttrium and calcium was investigated to improve the redox capacity and basicity of zirconia-supported catalysts in methanol APR [125]. Base Ni/ZrO_2 catalyst reported 48% of conversion and 40% hydrogen yield. Ce addition decreased the activity, in contrast with other works in the literature. Despite the improvement of Ni reducibility, Ce negatively influenced the quality of the surface basicity (decrease of weak basic sites, with the formation of intermediate strength ones). Therefore, it seemed that the basicity plays a more significant role than the redox properties. Ca and Y addition increased the total surface basicity equally, with the former acting mainly in the formation of weak basic centers, and the latter in the establishment of medium/strong basic centers. The Ca-doped catalyst showed better performance than the Y-doped one because strong basic sites can negatively affect the results by preventing the desorption of CO_2. Finally, increasing the Ca loading from 4% to 14% worsened the activity, likely due to the decrease of Ni surface area (despite the higher amount of weak and intermediate basic sites).

The addition of Ce is common on Zr support. We cite here its investigation on two examples, with Ni- and Pt-based catalysts. Bastan et al. investigated the effect of the Ce–Zr support composition for Ni-based catalysts prepared by co-precipitation for APR of glycerol [126]. XRD showed that the two oxides were present in a mixed form, not as separated clusters, and presented higher surface area than the single oxide support. Zr included in the Ce lattice lowered the crystallite size due to its lower ionic radius. The Ni reducibility changed in the mixed oxide, with the increasing of Zr loading leading to an increase of the reduction temperature peak, likely suggesting stronger metal-support interaction. Finally, the increase of Zr also allowed to increase the Ni dispersion. It is likely that this difference caused the increase of glycerol conversion for the mixed oxides, however the hydrogen selectivity decreased. The best catalyst ($Ni/Ce_{0.3}Zr_{0.7}O_2$) was tested also for stability with 25 h TOS. No drop in the conversion was reported; moreover, commonly deactivation mechanisms such as Ni re-oxidation and sintering were excluded.

The effect of cerium/zirconium molar ratio for Pt-based catalyst is studied in Ref. [127]. The activity and hydrogen selectivity were maximized when the Ce/Ce + Zr molar ratio was 0.4. The lowest CO concentration in this case suggests also more effective WGS. The authors reported that this ratio led to a higher abundance of oxygen vacancy sites which, being correlated with the platinum dispersion, may be considered the cause for the higher performance of this formulation thanks to strong metal-support interactions. Raman analysis was carried out to measure the defect sites. Mixed oxides have larger lattice strain and higher oxygen vacancy concentration, with the one at 0.4 ratio having the highest. H_2-TPR showed improved reducibility in the case of mixed oxides, ascribed to the higher oxygen mobility. Finally,

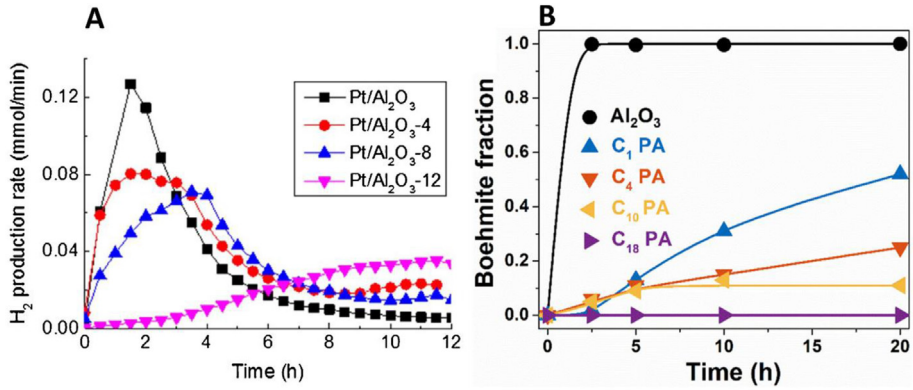

Fig. 18 – A: Use of silica deposition (from Ref. [123]) and B: alkyl phosphonate coating (Adapted with permission from Ref. [124]. Copyright 2018 American Chemical Society) as strategies to improve alumina stability under hydrothermal conditions.

the sample 0.4 showed also less sintering compared to Pt supported on only ceria or zirconia.

Larimi et al. investigated ternary Pt–Ce–Zr solid solutions prepared by controlled precipitation methods with different Ce/Zr ratio, looking at its influence on the oxidation state of Pt and its particle size (dispersion) [128]. The presence of a ternary solid solution was confirmed by XRD. When Ce/Zr ratio was equal to 1, the dispersion was the highest and it was the one with the highest hydrogen activity. Looking at the TOF, it was reported that face atoms (larger particles) are more active, while higher H_2 selectivity was obtained with the smallest particles. XPS analysis showed the electronic interaction between Pt, Ce and Zr through the increase of Pt binding energies. Electron withdrawing from Pt should cause the decrease of the Pt–CO binding, enhancing in this way the WGS. Furthermore, the catalyst was proven stable in the APR condition, without agglomeration of Pt.

Finally, Harju and coworkers reported a mild effect of zirconia particle size on butanol conversion, while the product distribution and the stability was negatively affected using bigger particles due to the onset of internal mass transport limitations [129]. In the 250–420 μm range, butyric acid selectivity increased, favoring the active metal (Rh) leaching and decreasing the hydrogen formation by favoring hydrogen-consuming reactions (e.g. hydrogenolysis).

Carbon

Several carbon supports (activated carbon, single and multi-walled carbon nanotubes, superdarco (i.e., methane and steam treated) carbon and graphene oxide) were studied for Pt-based materials [130]. Activated carbon reported the highest gas production among the supports while graphene oxide the highest hydrogen selectivity. Moreover, SWCNT performed better than MWCNT likely because of the larger pores that facilitate the reaction of large molecules present in the hydrolysate.

Wang et al. studied the influence of surface functional groups in MWCNT used as support for Pt based catalysts in ethylene glycol APR [131]. HNO_3 functionalization increased the Pt dispersion but decreased the turnover frequency. The authors ascribed this outcome to the presence of oxygen containing groups, which can create a competitive adsorption between water and ethylene glycol, due to the increase in hydrophilicity. An annealing treatment which removed these groups allowed to restore the original TOF.

Finally, it is worthy to cite the effect that the carbon support morphology can have on APR. Meryemoglu et al. looked at three ranges of activated carbon: < 88 μm, 177-88 μm, 177–250 μm [132]. Smaller particles had higher surface area and pore volume. Pt size was similar, so the difference can be ascribed only to the support. It was showed that activity increased with decreasing particle size, as well as for narrower size distribution. Kim et al. investigated the importance of the configuration of the support looking at 3-D and 2-D ordered mesoporous carbon with hollow- and rod-type configuration [133]. The order of hydrogen production was different from the order of the metal dispersion, highlighting the importance of the structure of the support. It was noted that 3-d ordered mesoporous carbon (OMC) allowed higher resistance towards sintering for the Pt particles; furthermore, the mesoporosity of hollow-type framework configuration favored the transport of reactant and products to and from the active sites, respectively.

Effect of the preparation method

The preparation of a catalyst involves different steps, and each of them can affect its final characteristics. First of all, the formation of the metal-support system is necessary. It may be carried out via impregnation, deposition, ion exchange, etc. During this stage, liquid/solid interfacial phenomena are important and can affect the behavior of the final catalyst. In the APR literature, most of the works deals with impregnation (wet or incipient wetness) and will not be reported in this paragraph, unless for the sake of comparison. Only limited information was reported on the procedures and methods themselves, since outside of the scope of the work. Then, the second stage involves (commonly) gas-solid reactions, firstly in the calcination (oxidation) step, and afterwards in the activation (hydrogenation, sulfidation)

step. The modifications caused by this second stage strongly influence the structure of the catalyst as obtained after the first stage [134]. This is the reason why both of them are analyzed in the following.

Step 1: formation of the metal-support system

Alternative methods to the traditional impregnation can contribute to increase the reducibility of the metal, facilitate alloy formation or the interaction between two metals in case of bi-metallic systems [135,136]. However, most of the time they are developed to increase the dispersion, so that a high metallic surface area available for the reaction can boost the productivity. For example, it was reported that silica-supported platinum catalysts prepared via ionic exchange (IE) showed higher metal dispersion (60%) than the ones prepared via incipient wetness impregnation (20%) [91]. This result allowed to nearly double the hydrogen yield. Analogously, urea matrix combustion method (UCM) compared with IWI for the APR of different polyols allowed higher dispersion and, as a consequence, higher hydrogen yield [44].

As far as the choice of the metal precursor is concerned, Lehnert and Claus evaluated the influence of different platinum precursors (amines, nitrates, sulfites) with IWI technique [88] They observed slight differences among the salts in terms of glycerol conversion and hydrogen selectivity, with tetrammine platinum (II)-nitrate giving the highest hydrogen rate of production.

Lemus et al. developed a method to synthesize stable Pt size-controlled nanoparticles [137]. The novelty consisted in synthesizing the metal nanoparticles in situ, in the presence of the support, therefore leading to the immobilization on it (contrarily to methods where the nanoparticles are first prepared and later deposited, ex situ). The authors used polyvinylpyrrolidone (PVP) and $NaBH_4$ as capping and reducing agent, respectively. Bigger particles were obtained by ex situ method, as well as with a reference method without PVP. However, the addition of PVP only after the contact with activated carbon led to a higher dispersion, as no competition was present between the nanoparticles and the capping agent.

Apart from the activity and selectivity, also the stability can be affected by the preparation method. El Doukkali et al. compared the preparation of Pt and Ni catalysts on alumina via incipient wetness impregnation (IWI) and sol-gel method under basic conditions (SGB) [138]. Sol-gel created a material with higher surface area (375 vs. 140 m^2/g) and pore volume (0.43 vs. 0.23 cm^3/g). The basic agent leads to spherical cluster formation and a spongy material. The pore volume decreased in SGB after adding the metal, likely because they were incorporated in the pores network, while they were mainly in the outer surface in the case of IWI. SGB also increased the interaction of Ni with the support (leading to Ni aluminate) favoring the dispersion. The latter was confirmed by broader peaks in XRD. SGB method also stabilized Pt particles which otherwise sintered during the reduction step when prepared via IWI. The carbon conversion to gas increased with SGB catalysts. In a subsequent work, the authors added also the study of sol-gel preparation under acidic conditions (SGA) [139]. The differences in the preparation method are reported in Fig. 19-A. SGA led to a material with fibrous and laminated morphology and high surface area, allowing an effective dispersion of Pt and Ni: the modification in the morphology facilitated adsorption of reactant and desorption of the products, whereas the higher dispersion increased the activity. The catalysts prepared by SGA had 50% higher surface area than IWI, but 50% lower than SGB. Looking at the performance, the activity was in the same trend (Fig. 19-B). Finally, SGB led to catalysts more resistant to sintering compared to the ones prepared by SGA.

The same research group reviewed the deactivation mechanisms for the catalysts subjected to APR in Ref. [141]. No leaching was reported for Pt, Ni and PtNi catalysts both at 230 and 250 °C. The textural characterization showed that the decrease of surface area involved the materials prepared by sol-gel routes more than the ones by IWI. XRD showed higher transition to boehmite in the supports synthesized by sol-gel, likely due to their higher surface area that facilitates the incorporation of water molecule. Ni sintering occurred, and it was higher for those prepared by IWI. However, contrarily to literature, Pt did not sinter. XPS showed that monometallic Ni completely re-oxidized, while it was metallic only in the 11–25% in the bimetallic case (lower for the sol-gel because of the higher dispersion). Pt remained in the metallic form after the reaction. Finally, temperature programmed oxidation (TPO) showed the presence of carbonaceous species adsorbed on the catalysts.

Roy et al. compared sol-gel method and solution combustion synthesis (SCS) combined with wet impregnation method for Ni/CeO_2 catalysts [142]. The first one showed higher carbon conversion to gas and hydrogen selectivity, ascribed to the growth of Ni nanoparticles prepared by SCS during the reaction. Analogously, the same research group looked at Ni/γ-Al_2O_3 catalysts, revealing that in this case SCS samples outperformed the ones prepared by sol-gel in terms of activity (i.e., ethanol conversion), hydrogen selectivity and TOF [143,144]. The extensive structural and superficial characterization showed that it was not only due to the smaller particles obtained by SCS. In fact, SCS sintered in a lower extent, produced less coke and bulk spinel formation (promoting WGS) than SG.

Other examples of better dispersion of the active phase in the case of sol-gel route compared to impregnation are reported in Ref. [145].

Step 2: thermal treatment and activation

Following the preparation steps, two further phases are commonly involved, calcination and reduction.

Callison and coworkers used a colloidal synthesis procedure for the preparation of platinum particles [96]. The synthesis procedure was optimized varying the concentration of $NaBH_4$ (reducing agent), reduction time of Pt precursor and immobilization time on the support. Afterwards, the reduction temperature was varied from 25 °C to 90 °C to change the particle size. As expected, it was shown that it increased with the increase of reduction temperature.

Morales-Marin et al. used bulk nickel-aluminate catalysts reduced at different temperatures from 300 to 850 °C [146]. The authors observed that increasing the reduction

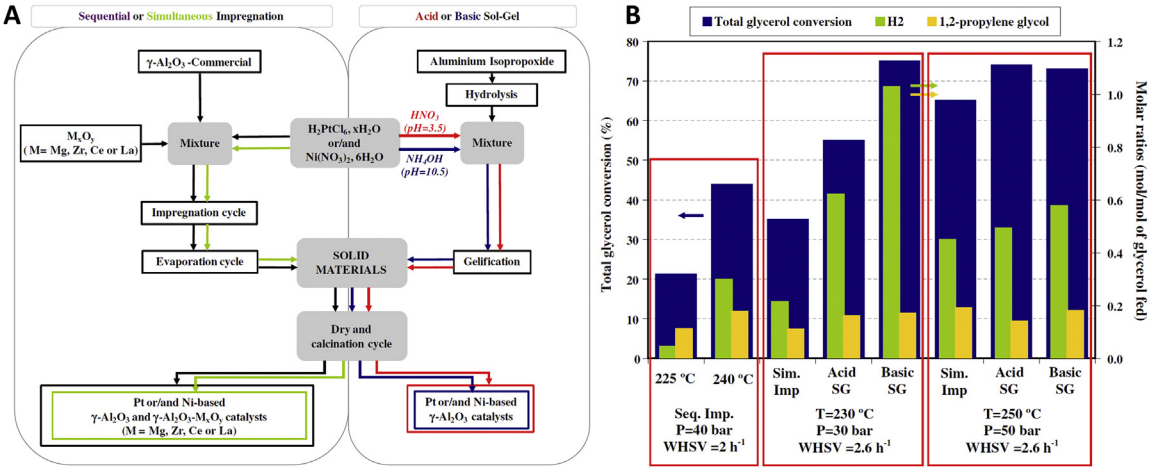

Fig. 19 – A: Preparation method followed for the synthesis of Pt and Ni supported catalysts and B: its effect on the APR of glycerol using Pt–Ni/γ-Al_2O_3 catalyst (from Ref. [140]).

temperature had a two-fold effect and the results of the catalytic tests are reported in Fig. 20. On one side, the nickel dispersion increased because its migration from the spinel structure to the surface is favored. On the other hand, both surface acidity and (to a greater extent) basicity increased. Up to 450 °C, less than 5% conversion was reported due to the absence of the Ni^0 active site. In this range, hydroxyacetone was the main product, deriving from dehydration reactions catalyzed by Lewis acid sites. As a matter of fact, this outcome is properly exploited in works where the aim is the hydrogenolysis of glycerol and the production of C3 products [147]. From 600 to 850 °C, the glycerol conversion and gas production gradually increased, with the maximum hydrogen yield at 850 °C. However, hydrogen selectivity partially reduced due to its consumption in parallel reactions. Nickel oxidation and sintering were identified as the leading cause for catalyst deactivation, while leaching and coke were excluded. Interestingly, sintering was observed mainly for the larger particles, in contrast with previous literature [102].

El Doukkali et al. evaluated the influence of calcination temperature (550–750 °C) on the stability of alumina and Ni/Pt particles [148]. The Pt particle size was similar, independently from the calcination temperature. Moreover, in one case the active sites were incorporated during the SGB synthesis of alumina; in the second case, they were impregnated by IWI after sol-gel alumina preparation (SGI). Ni particles were bigger for SGI, but less sensitive to the calcination temperature, while sintering occurred with SGB, causing more deactivation. Bigger particles are more resistant to sintering (4-fold increase for SGB, two-fold for SGI) and re-oxidation, which are common deactivation causes for Ni. Increasing the calcination temperature decreased the activity but increased the stability.

Irmak et al. studied different preparation and reduction methods of platinum on activated carbon, alumina and titania by IWI [149]. Thermal treatments were carried out under hydrogen and nitrogen: in the latter case the activity improved thanks to the lower particle size. Afterwards, reducing the precursor chemically (using $NaBH_4$) rather than thermally, further improved the catalyst activity, thanks to the fast reduction process when it is added dropwise to the solution.

Innovative synthesis for APR

Novel techniques, even if not applied for APR yet, are worthy to be mentioned. Keshavarz et al. used microemulsion systems to prepare Pt and Re based catalysts with controlled particle size for heptane reforming [150]. Two different microemulsions, neutral and acidic, were prepared. Re particle size was larger for neutral microemulsions, while Pt particle size was larger for acidic microemulsions, as well as for Pt–Re. Interestingly, the nature of the microemulsions did not affect the final acidic properties of the supported catalyst.

The influence of surfactants on the synthesis of platinum nanoparticles via microemulsion method [151] was studied as well. In this method, nanosized water droplets in which the

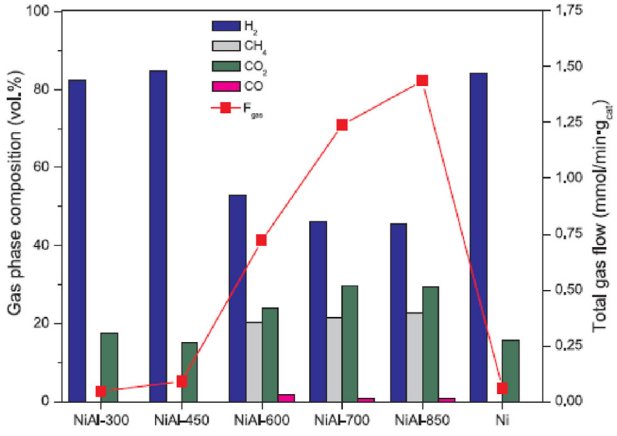

Fig. 20 – Influence of the reduction temperature of bulk nickel aluminate on the gas phase composition and production from glycerol APR. Reaction conditions: 250 °C/45 bar, 10 wt% glycerol solution, 0.2 mL/min, 0.5 g catalyst (from Ref. [146]).

metal salt is dissolved work as a nanosized reactor during the reduction while dispersed into a continuous oil phase. Four surfactants were used: Sodium 1,4-bis(2-ethylhexoxy)-1,4-dioxobutane-2-sulfonate (AOT), cetyltrimethylammonium-bromide (CTAB), poly(oxyethylene) sorbitanmonooleate (Tween80) and poly(ethylene glycol) p-(1,1,3,3-tetramethylbutane)-phenyl ether (TX-100). It was reported that ionic surfactants allowed producing smaller nanoparticles than non-ionic ones (AOT < CTAB < Tween80 < T-X-100, i.e., anionic surfactant < cationic surfactant < nonionic surfactant) thanks to the influence of the different head group charge, as it affects the dynamic process of collision, nucleation and growth of the droplets. Other examples of microemulsion synthesis of nanoparticles can be found in Ref. [152], where the authors prepared NiPt bimetallic nanoparticles for methane dry reforming.

Finally, Roy et al. reported the use of a radio-frequency plasma treatment to modify the surface of a Ni/alumina catalyst [153]. The plasma modification mainly influenced the metal-support interaction leading to a higher dispersion of the metal, leading to an increase of the catalytic activity.

In Table 4 the influence of preparation method reported in the chapter is summarized. Among the others, sol-gel methods seemed particularly interesting for their simplicity and possibility to increase the dispersion; as usual, the trade-off is reported being affected the stability of the catalyst, which is particularly sensitive when alumina support is used. Once the support-active metal system is formed, the conditions used in the calcination and reduction steps can still play a role in modifying the final catalyst properties due to its dynamic structure.

Table 4 – Influence of preparation method. IWI: incipient wetness impregnation; IE: ionic exchange; SGB: sol-gel basic; SGA: sol-gel acid; UCM: urea matrix combustion; SCS: solution combustion synthesis.

Ref.	System	Preparation mode	Main outcome
[91]	Pt/SiO_2	IE vs. IWI	IE dispersion 60% - IWI dispersion 20%; doubling of H_2 yield
[44]	Pt-based/Al_2O_3	IWI vs UCM	UCM led higher dispersion
[88]	Pt/Al_2O_3	IWI - Influence of platinum precursors	7.6 mmol H_2/min·g_{cat} hydrogen rate production for catalyst prepared with tetrammine platinum (II) nitrate
[138]	Pt–Ni/Al_2O_3	IWI vs SGB	SGB higher dispersion and resistance to sintering during the reduction step
[139]	Pt–Fe,-Co,-Ni/Al_2O_3	IWI vs SGB vs SGA	Activity ranking SGB > SGA > IWI; SGB more sintering resistant than SGA
[141]	Pt–Ni/Al_2O_3	IWI vs SG	SG more prone to boehmite transition; Ni re-oxidized in SG because of the higher dispersion
[135]	Pt–Ni/alumina nanofibers	Sequential vs co-impregnation	Co-impregnation favored alloy formation, reducibility and resistance to CO binding
[136]	Pt–Ni/hydrotalcite	Surface organometallic chemistry	High interaction between Pt and Ni
[137]	Pt/C	In situ nanoparticles formation	In situ 2.5 nm vs ex situ 4.5 nm
[142]	Ni/CeO_2	SG vs SCS + WI	SCS formed smaller particles, more resistant to sintering and with less coke deposition
[150]	Pt.Re/Al_2O_3	Acidic and neutral microemulsion	Acidic favored Re dispersion, neutral favored Pt dispersion
[151]	Pt/α-Al_2O_3	Influence of surfactants	Particle size ranking: AOT < CTAB < Tween80 < T-X-100
[96]	Pt/Al_2O_3	Influence of reduction temperature (25–90 °C)	The particle size increased with the reduction temperature
[146]	$NiAl_2O_4$	Influence of reduction temperature (300–850 °C)	Max H_2 yield at 850 °C due to the combination of increased Ni dispersion and basicity
[148]	Pt–Ni/Al_2O_3	Influence of calcination temperature (550–750 °C)	Pt: insensitive; Ni: increasing the calcination temperature decreased the activity whereas increasing the stability
[149]	Pt/C, Pt/Al_2O_3, Pt/TiO_2	Influence of reduction methods	Chemical reduction improved the catalyst activity

Perspectives

Catalytic perspectives

In the present work we collected the efforts of several research groups whose aim is the design of an effective catalyst for APR. The scientific outcomes have been classified according to the effect of three main steps: choice of the preparation method, choice of the metal, choice of the support. It is important to observe that the reality is not as simple as reported, and the boundaries are much more flexible. For example, glycerol conversion rate decreases in the order TiO_2 > ZrO_2 > $CeZrO_2$ > CeO_2 on Pt, but the ranking changes into TiO_2 > $CeZrO_2$ > ZrO_2 > CeO_2 on Pt-Re [154]. It means that changing the metal, apparently also changed the effect of the support. Similarly, changing the support affected also the ranking between preparation methods, as reported in the works of Roy et al., where CeO_2 was more active prepared by sol-gel than SCS, but viceversa for Al_2O_3 [142–144]. Notwithstanding, an ideal combination of these ingredients may be proposed at the end of the present work. The active elements should likely rely on bimetallic systems. Nowadays, platinum appears inevitable due to its peculiar characteristics. Despite of its cost, the key point refers to avoiding its deactivation, which seems an affordable task, at least with model compounds. From the available literature, it should be accompanied by a promoter to increase mainly its water gas shift

activity. Among the others, Re and Fe seemed the most suitable. If the metals could explicate the WGS effectively, the support may just play the role of dispersive medium. For this reason, mesoporous carbon, thanks to its inert behavior with respect to the aqueous phase and controlled pore size, may be a suitable support. Finally, the coupling of in situ formation of nanoparticles and their activation by chemical reduction methods could be a preparation method able to guarantee high dispersion and stability of the active phase.

Apart from the characteristics of the catalyst, the hydrogen yields strongly depend on the nature of the substrate, due to severe selectivity issues that arise with the increasing complexity of the molecule. In other words, we can expect high yield for small molecules (methanol, ethylene glycol, glycolic acid), while it will decrease for glycerol, xylitol or sorbitol. For example, we observed with glycolic acid 65% hydrogen yield with Pt/C while it was 38% for sorbitol, at iso-conversion conditions [11,12].

However, looking also to an industrial application, the TOF values could be even more interesting. Lange reported that its value should be in the range 0.033–16.7 tons of product per ton of catalyst per min [155]. For Pt-based catalysts, for example, it could reach 3 min^{-1} [95,156] and this figure is promising for the future. However, it remains to be proofed also for more complex systems (see paragraph 6.2). For example, Pt–Rh catalyst applied to the APR of pure glycerol showed 83.5% glycerol conversion and 89% hydrogen selectivity, while these values dropped respectively to 43.1% and 39% for crude glycerol [36].

The future research should focus on each of the three cited topics to improve the performance of the catalytic system in the APR scenario. In the following, some points worthy of consideration are reported.

In the field of the preparation method, innovative aspects such as the effect of the orientation of the active sites compared with unoriented Pt materials on graphene prepared by IWI, showed that the oriented material reported 2 order of magnitude higher catalytic activity expressed as TOF than unoriented ones [157]. Moreover, novel preparation techniques for bimetallic catalysts may be developed to handle the harsh conditions of the reduction treatment and reaction (for example, leading to stronger metal-support interactions) and stabilize the bimetallic clusters.

Apart from experimental testing, the rational design of heterogeneous catalysts, thanks to the use of multiple tools such as DFT and micro-kinetic models, should benefit from further understanding of the reaction mechanism and lead to more effective catalysts. In this sense, the fact that APR occurs in liquid conditions is an obstacle, since the presence of a solvent that interacts with reagents, intermediates and products, modifies the energetic and reaction pathways [158]. The aqueous environment also affects the common knowledge in the reactivity of the catalytic system. It means that typical gas-phase WGS catalysts, such as Cu and CeO_2, are not trivially effective catalysts also in the liquid phase.

The use of a second metal to improve the activity, selectivity and stability of the primary active site has been proved to be commonly effective. However, despite the achievements, the complexity of the systems often requires further efforts. For example, it has been reported that the bimetallic structures modify under the reaction conditions: therefore, the development of in situ characterization techniques is necessary. Furthermore, new and cheap materials, such as tungsten, can be promising for future applications in the field [159].

Much work needs to be done also on the support side, to clarify its role in the reactivity of the total system. For this reason, understanding phenomena such as charge transfer, spillover and perimeter activation may help in the design of new catalysts with tailored properties [160].

Apart from the ones cited in this work, the catalyst will face new challenges when it goes towards the use of real wastewater streams. In fact, the complexity of the multi-components mixture may rise competitive adsorption phenomena [12]; moreover, the presence of inorganics or high molecular weight organics can lead to fast deactivation [161].

Focusing on the latter, also the studies with model compounds, despite trying to assess the stability, are often referred to short runs, and so insufficient to probe the stability as demanded by chemical industry. Furthermore, studies on catalyst synthesis scalability and regeneration protocols should be developed.

Technological perspectives

The literature cited herein applies the APR to simple model compounds, since its aim is the study and development of effective catalysts. However, the application of APR is devoted to the valorization of complex multicomponent mixtures, as it is the case of biorefinery wastewater streams. For this reason, in the last decade, the research started to investigate such feedstocks. Due to is versatility, APR could be applied to treat the water fractions derived from lignocellulosic biomass processing (e.g. not fermentable sugars post hydrolysis, aqueous phase from pyrolysis and hydrothermal liquefaction, etc.), aqueous effluents from food processing (e.g. breweries, cheese factories, etc.), crude glycerol from the biodiesel sector, and others [162]. Most of these works used simple catalytic systems (typically monometallic platinum catalysts), however they provide a range of hydrogen productivity into a more industrially relevant environment. For example, referring to the brewery wastewater, it was estimated that about 294 mL H_2/g COD could be produced via APR, while anaerobic digestion could reach roughly half (150 mL H_2/g COD) production [8]. Under the economic point of view, Larimi and coworkers showed that glycerol APR has lower production cost than glycerol steam reforming (3.55 vs 3.65 $/Kg), and this is competitive with other technologies which aim at a renewable hydrogen production (such as biomass gasification, dark fermentation, solar thermal electrolysis) [163,164]. Globally, the application of APR at industrial scale can be competitive if the cost of the feedstock is competitive as well. As a matter of fact, it can account for most of the production cost (e.g. up to 92% in the case of hydrogen from sorbitol syrup [165]).

Conclusion

Aqueous phase reforming has been conceptualized as a strategic process for the valorization of biomass-derived compounds for hydrogen production. Since 2002, most of the literature focused on the pursuit of the optimal catalytic

system that maximizes activity, selectivity and stability. Despite the efforts, the complexity of the reaction and the intercorrelation among the variables hindered, at the moment, the possibility to turn this process from the laboratory to the industrial scale. The aim of the present review was reporting, in a comprehensive way, the influence of several variables which can affect each of the three figures.

Scope of the preparation method was mainly maximizing the dispersion to increase the number of available active sites. Alternative methods to the conventional impregnation techniques, such as ionic exchange, sol-gel and microemulsions reached this aim. Furthermore, they modified the electronic properties of the metal, for example via alloy formation or strong metal-support interaction, which in turn affected the reducibility, the tendency to CO binding or sintering.

Theoretical investigation and first-principle methods, such as DFT, showed the intrinsic predisposition of metals to activate one or another pathway. Among the others, Pt showed higher tendency to C–C cleavage than C–O cleavage, maximizing the hydrogen production. The use of a promoter allowed to exalt or suppress some characteristic features of the monometallic catalytic form. Different promotion phenomena were reported. Ensemble (or geometric) effects were shown when Sn addition hindered the CO methanation on Ni-based systems; stabilizing effects have been attributed to Ru and Rh when protected Pt from coke deposition and sulfur poisoning, respectively; ligand (or electronic) effects were largely reported when the promoters decreased the interaction between carbon monoxide and Pt active site, favoring WGS (Re, Co, Fe, Mo). Overall, it has been widely documented that the second metal can tune the catalyst modifying the binding energy with reactants, intermediates or products, improving the reducibility of the first metal or its dispersion, changing the surface acid-base properties. Each of these modifications can have a different degree of importance, and it depends on the catalytic system as a whole. For example, it seemed that increasing the metal surface area is more important than the increase of (weak) basic properties, which in turn play a more important role than the metal reducibility. Trade-off is ubiquitous in the design of the optimal catalyst, as the example of the choice of the metal particles exemplifies. Despite results are not totally coherent, we can assume that the size of the particles mainly affects the selectivity, with the smaller ones favoring dehydrogenation and C–C cleavage, while the bigger ones favoring dehydration and methanation; if the conversion is affected, this is higher for larger particles, which caused less coke deposition as well.

Finally, the choice of the support mainly affected the dispersion thanks to its surface area and favored (or not) dehydration acid-catalyzed reactions. Basic character of the support was linked to the promotion of water gas shift and, in turn, to higher hydrogen production. The hydrothermal stability, such as the case of Al_2O_3 and MgO, is a severe issue that can be overcome properly modifying the surface composition and morphology.

Despite several challenges remain to be tackled, we strongly believe that the developments in the field of catalysis through innovative preparation methods, rational design and in situ characterization techniques can pave the way to the synthesis of effective catalysts for aqueous phase reforming and sustainable hydrogen production.

Declaration of competing interest

The authors declare that they have no known competing financial interests or personal relationships that could have appeared to influence the work reported in this paper.

Acknowledgement

The project leading to this research has received funding from the European Union's Horizon 2020 research and innovation program under grant agreement N 764675. Gianna Moscoso Thompson is gratefully acknowledged for the graphical abstract artwork.

REFERENCES

[1] de Jong E, Langeveld H, van Ree R. IEA Bioenergy 2013:28. http://www.biorefinery.nl/fileadmin/biorefinery/docs/Brochure_Totaal_definitief_HR_opt.pdf.
[2] Leoneti AB, Aragão-Leoneti V, de Oliveira SVWB. Renew Energy 2012;45:138–45. https://doi.org/10.1016/j.renene.2012.02.032.
[3] Chiaramonti D, Prussi M, Buffi M, Rizzo AM, Pari L. Appl Energy 2017;185:963–72. https://doi.org/10.1016/j.apenergy.2015.12.001.
[4] Panisko E, Wietsma T, Lemmon T, Albrecht K, Howe D. Biomass and Bioenergy 2015;74:162–71. https://doi.org/10.1016/j.biombioe.2015.01.011.
[5] Cortright RD, Davda RR, Dumesic JA. Nature 2002;418:964–7. https://doi.org/10.1038/nature01009.
[6] Valenzuela MB, Jones CW, Agrawal PK. Energy Fuels 2006;20:1744–52. https://doi.org/10.1021/ef060113p.
[7] Pipitone G, Tosches D, Bensaid S, Galia A, Pirone R. Catal Today 2018;304:153–64. https://doi.org/10.1016/j.cattod.2017.09.047.
[8] Oliveira AS, Baeza JA, Calvo L, Alonso-Morales N, Heras F, Rodriguez JJ, Gilarranz MA. Appl Catal B Environ 2019;245:367–75. https://doi.org/10.1016/j.apcatb.2018.12.061.
[9] Oliveira AS, Baeza JA, Calvo L, Alonso-Morales N, Heras F, Lemus J, Rodriguez JJ, Gilarranz MA. Environ Sci Water Res Technol. 2018;4:1979–87. https://doi.org/10.1039/c8ew00414e.
[10] Saenz de Miera B, Oliveira AS, Baeza JA, Calvo L, Rodriguez JJ, Gilarranz MA. J Clean Prod 2020;252:119849. https://doi.org/10.1016/j.jclepro.2019.119849.
[11] Pipitone G, Zoppi G, Frattini A, Bocchini S, Pirone R, Bensaid S. Catal Today 2020;345:267–79. https://doi.org/10.1016/j.cattod.2019.09.031.
[12] Pipitone G, Zoppi G, Bocchini S, Rizzo AM, Chiaramonti D, Pirone R, Bensaid S. Catal Today 2020;345:237–50. https://doi.org/10.1016/j.cattod.2019.09.040.
[13] Pipitone G, Zoppi G, Ansaloni S, Bocchini S, Deorsola FA, Pirone R, Bensaid S. Chem Eng J 2019;377:120677. https://doi.org/10.1016/j.cej.2018.12.137.
[14] Zoppi G, Pipitone G, Gruber H, Weber G, Reichhold A, Pirone R, Bensaid S. Catal Today 2020. https://doi.org/10.1016/j.cattod.2020.04.024.

[15] Davda RR, Shabaker JW, Huber GW, Cortright RD, Dumesic JA. Appl Catal B Environ 2005;56:171–86. https://doi.org/10.1016/j.apcatb.2004.04.027.
[16] Chen G, Li W, Chen H, Yan B. J Zhejiang Univ A 2015;16:491–506. https://doi.org/10.1631/jzus.A1500023.
[17] Coronado I, Stekrova M, Reinikainen M, Simell P, Lefferts L, Lehtonen J. Int J Hydrogen Energy 2016;41:11003–32. https://doi.org/10.1016/j.ijhydene.2016.05.032.
[18] Vaidya PD, Lopez-Sanchez JA. Chemistry 2017;2:6563–76. https://doi.org/10.1002/slct.201700905.
[19] El Doukkali M, Iriondo A, Gandarias I. Mol Catal 2020;490:110928. https://doi.org/10.1016/j.mcat.2020.110928.
[20] Davda RR, Alcalá R, Shabaker J, Huber G, Cortright RD, Mavrikakis M, Dumesic JA. Stud Surf Sci Catal 2003;145:79–84. https://doi.org/10.1016/s0167-2991(03)80168-4.
[21] Alcalá R, Mavrikakis M, Dumesic JA. J Catal 2003;218:178–90. https://doi.org/10.1016/S0021-9517(03)00090-3.
[22] Gursahani KI, Alcalá R, Cortright RD, Dumesic JA. Appl Catal A Gen 2001;222:369–92. https://doi.org/10.1016/S0926-860X(01)00844-4.
[23] Sutton JE, Panagiotopoulou P, Verykios XE, Vlachos DG. J Phys Chem C 2013;117:4691–706. https://doi.org/10.1021/jp312593u.
[24] Schimmenti R, Cortese R, Godina L, Prestianni A, Ferrante F, Duca D, Murzin DY. J Phys Chem C 2017;121:14636–48. https://doi.org/10.1021/acs.jpcc.7b03716.
[25] Faheem M, Saleheen M, Lu J, Heyden A. Catal Sci Technol 2016;6:8242–56. https://doi.org/10.1039/c6cy02111e.
[26] Xie T, Hare BJ, Meza-Morales PJ, Sievers C, Getman RB. J Phys Chem C 2020;124:19015–23. https://doi.org/10.1021/acs.jpcc.0c03717.
[27] Chiu CC, Genest A, Rösch N. Top Catal 2013;56:874–84. https://doi.org/10.1007/s11244-013-0051-0.
[28] Vannice MA. J Catal 1977. https://doi.org/10.1016/0021-9517(77)90031-8.
[29] Liu B, Greeley J. Phys Chem Chem Phys 2013;15:6475–85. https://doi.org/10.1039/c3cp44088e.
[30] Davda RR, Shabaker JW, Huber GW, Cortright RD, Dumesic JA. Appl Catal B Environ 2003;43:13–26. https://doi.org/10.1016/S0926-3373(02)00277-1.
[31] Dal Santo V, Gallo A, Naldoni A, Guidotti M, Psaro R. Catal Today 2012;197:190–205. https://doi.org/10.1016/j.cattod.2012.07.037.
[32] Huber GW, Shabaker JW, Dumesic JA. Science 2003;300:2075–7. https://doi.org/10.1126/science.1085597.
[33] Shabaker JW, Huber GW, Dumesic JA. J Catal 2004;222:180–91. https://doi.org/10.1016/j.jcat.2003.10.022.
[34] Huber GW, Shabaker JW, Evans ST. J.A. Dumesic 2006;62:226–35. https://doi.org/10.1016/j.apcatb.2005.07.010.
[35] Godina LI, Kirilin AV, Tokarev AV, Simakova IL, Murzin DY. Ind Eng Chem Res 2018;57:2050–67. https://doi.org/10.1021/acs.iecr.7b04937.
[36] Larimi A, Khorasheh F. Int J Hydrogen Energy 2019;44:8243–51. https://doi.org/10.1016/j.ijhydene.2019.01.251.
[37] Larimi AS, Kazemeini M, Khorasheh F. Int J Hydrogen Energy 2016;41:17390–8. https://doi.org/10.1016/j.ijhydene.2016.08.006.
[38] Guo Y, Azmat MU, Liu X, Wang Y, Lu G. Appl Energy 2012;92:218–23. https://doi.org/10.1016/j.apenergy.2011.10.020.
[39] Oliveira ÉV, Seixas ACM, Jordão E. Can J Chem Eng 2017;95:2018–23. https://doi.org/10.1002/cjce.22826.
[40] Guo Y, Liu X, Wang Y. Ind Eng Chem Res 2019;58:2749–58. https://doi.org/10.1021/acs.iecr.8b05774.
[41] Kim MC, Kim TW, Kim HJ, Kim CU, Bae JW. Renew Energy 2016;95:396–403. https://doi.org/10.1016/j.renene.2016.04.020.
[42] Yfanti VL, Vasiliadou ES, Sklari S, Lemonidou AA. J Chem Technol Biotechnol 2017;92:2236–45. https://doi.org/10.1002/jctb.5282.
[43] Soares AVH, Perez G, Passos FB. Appl Catal B Environ 2016;185:77–87. https://doi.org/10.1016/j.apcatb.2015.11.003.
[44] Dosso LA, Vera CR, Grau JM. Int J Hydrogen Energy 2017;42:18853–64. https://doi.org/10.1016/j.ijhydene.2017.06.100.
[45] Pendem C, Sarkar B, Siddiqui N, Konathala LNS, Baskar C, Bal R. ACS Sustain Chem Eng 2018;6:2122–31. https://doi.org/10.1021/acssuschemeng.7b03512.
[46] Bossola F, Pereira-Hernández XI, Evangelisti C, Wang Y, Dal Santo V. J Catal 2017;349:75–83. https://doi.org/10.1016/j.jcat.2017.03.002.
[47] Kim H, Ju H, Kim T, Jeong K, Chae H, Jeong S, Lee C, Kim C. Int J Hydrogen Energy 2012;37:8310–7. https://doi.org/10.1016/j.ijhydene.2012.02.160.
[48] Kaya B, Irmak S, Hasanoglu A, Erbatur O. Int J Hydrogen Energy 2015;40:3849–58. https://doi.org/10.1016/j.ijhydene.2015.01.131.
[49] Stanley JNG, Benndorf P, Heinroth F, Masters AF, Maschmeyer T. RSC Adv 2014;4:28062–71. https://doi.org/10.1039/c4ra03474k.
[50] Lei Y, Lee S, Bin Low K, Marshall CL, Elam JW. ACS Catal 2016;6:3457–60. https://doi.org/10.1021/acscatal.6b00963.
[51] Dietrich PJ, Lobo-Lapidus RJ, Wu T, Sumer A, Akatay MC, Fingland BR, Guo N, Dumesic JA, Marshall CL, Stach E, Jellinek J, Delgass WN, Ribeiro FH, Miller JT. Top Catal 2012;55:53–69. https://doi.org/10.1007/s11244-012-9775-5.
[52] Dietrich PJ, Wu T, Sumer A, Dumesic JA, Jellinek J, Delgass WN, Ribeiro FH, Miller JT. Top Catal 2013;56:1814–28. https://doi.org/10.1007/s11244-013-0115-1.
[53] Liu B, Zhou M, Chan MKY, Greeley JP. ACS Catal 2015;5:4942–50. https://doi.org/10.1021/acscatal.5b01127.
[54] Dietrich PJ, Sollberger FG, Akatay MC, Stach EA, Delgass WN, Miller JT, Ribeiro FH. Appl Catal B Environ 2014;156–157:236–48. https://doi.org/10.1016/j.apcatb.2014.03.016.
[55] Dietrich PJ, Akatay MC, Sollberger FG, Stach EA, Miller JT, Delgass WN, Ribeiro FH. ACS Catal 2014;4:480–91. https://doi.org/10.1021/cs4008705.
[56] Wang X, Li N, Pfefferle LD, Haller GL. Catal Today 2009;146:160–5. https://doi.org/10.1016/j.cattod.2009.02.010.
[57] Jeon S, Park YM, Saravanan K, Han GY, Kim BW, Lee JB, Bae JW. Int J Hydrogen Energy 2017;42:9892–902. https://doi.org/10.1016/j.ijhydene.2017.01.221.
[58] De Vlieger DJM, Mojet BL, Lefferts L, Seshan K. J Catal 2012. https://doi.org/10.1016/j.jcat.2012.05.019.
[59] He C, Zheng J, Wang K, Lin H, Wang JY, Yang Y. Appl Catal B Environ 2015;162:401–11. https://doi.org/10.1016/j.apcatb.2014.07.012.
[60] Rahman MM, Church TL, Variava MF, Harris AT, Minett AI. RSC Adv 2014;4:18951–60. https://doi.org/10.1039/c4ra00355a.
[61] Tupy SA, Karim AM, Bagia C, Deng W, Huang Y, Vlachos DG, Chen JG. ACS Catal 2012;2:2290–6. https://doi.org/10.1021/cs3004227.
[62] Salciccioli M, Vlachos DG. ACS Catal 2011;1:1246–56. https://doi.org/10.1021/cs2003593.
[63] Simonetti DA, Kunkes EL, Dumesic JA. J Catal 2007;247:298–306. https://doi.org/10.1016/j.jcat.2007.01.022.
[64] Kunkes EL, Simonetti DA, Dumesic JA, Pyrz WD, Murillo LE, Chen JG, Buttrey DJ. J Catal 2008;260:164–77. https://doi.org/10.1016/j.jcat.2008.09.027.

[65] Wei Z, Karim A, Li Y, Wang Y. ACS Catal 2015;5:7312–20. https://doi.org/10.1021/acscatal.5b01770.
[66] King DL, Zhang L, Xia G, Karim AM, Heldebrant DJ, Wang X, Peterson T, Wang Y. Appl Catal B Environ 2010;99:206–13. https://doi.org/10.1016/j.apcatb.2010.06.021.
[67] Grabow LC, Gokhale AA, Evans ST, Dumesic JA, Mavrikakis M. J Phys Chem C 2008;112:4608–17. https://doi.org/10.1021/jp7099702.
[68] Ciftci A, Ligthart DAJM, Sen AO, Van Hoof AJF, Friedrich H, Hensen EJM. J Catal 2014;311:88–101. https://doi.org/10.1016/j.jcat.2013.11.011.
[69] Zhang L, Karim AM, Engelhard MH, Wei Z, King DL, Wang Y. J Catal 2012;287:37–43. https://doi.org/10.1016/j.jcat.2011.11.015.
[70] Ciftci A, Michel DAJ, Hensen EJM. Appl Catal B Environ 2015;174–175:126–35. https://doi.org/10.1016/j.apcatb.2015.02.027.
[71] Kirilin AV, Tokarev AV, Manyar H, Hardacre C, Salmi T, Mikkola JP, Murzin DY. Catal Today 2014;223:97–107. https://doi.org/10.1016/j.cattod.2013.09.020.
[72] Rahman MM. Catal Lett 2020;150:2674–87. https://doi.org/10.1007/s10562-020-03167-2.
[73] Zhang J, Xu N. Catalysts 2020;10. https://doi.org/10.3390/catal10010054.
[74] Luo N, Ouyang K, Cao F, Xiao T. Biomass and Bioenergy 2010;34:489–95. https://doi.org/10.1016/j.biombioe.2009.12.013.
[75] Tao J, Hou L, Yan B, Chen G, Li W, Chen H, Cheng Z, Lin F. Energy Fuels 2020;34:1153–61. https://doi.org/10.1021/acs.energyfuels.9b02149.
[76] Guo Y, Liu X, Azmat MU, Xu W, Ren J, Wang Y, Lu G. Int J Hydrogen Energy 2011;37:227–34. https://doi.org/10.1016/j.ijhydene.2011.09.111.
[77] Tuza PV, Manfro RL, Ribeiro NFP, Souza MMVM. Renew Energy 2013;50:408–14. https://doi.org/10.1016/j.renene.2012.07.006.
[78] Manfro RL, Pires TPMD, Ribeiro NFP, Souza MMVM. Catal Sci Technol 2013;3:1278–87. https://doi.org/10.1039/c3cy20770f.
[79] Rahman MM. Int J Hydrogen Energy 2015;40:14833–44. https://doi.org/10.1016/j.ijhydene.2015.09.015.
[80] Park YH, Kim JY, Moon DJ, Park NC, Kim YC. Res Chem Intermed 2015;41:9603–14. https://doi.org/10.1007/s11164-015-2020-7.
[81] Liu S, Tamura M, Shen Z, Zhang Y, Nakagawa Y, Tomishige K. Catal Today 2018;303:106–16. https://doi.org/10.1016/j.cattod.2017.07.025.
[82] Espinosa-Moreno F, Balla P, Shen W, Chavarria-Hernandez JC, Ruiz-Gómez M, Tlecuitl-Beristain S. Catalysts 2018;8. https://doi.org/10.3390/catal8120613.
[83] Sinfelt JH. Adv Catal 1973. https://doi.org/10.1016/S0360-0564(08)60299-0.
[84] Gogoi P, Kanna N, Begum P, Deka RC, Satyanarayana CVV, Raja T. ACS Catal 2020;10:2489–507. https://doi.org/10.1021/acscatal.9b04063.
[85] Reynoso AJ, Ayastuy JL, Iriarte-velasco U, Gutiérrez-ortiz MA, Technologies C. Appl Catal B Environ 2018;239:86–101. https://doi.org/10.1016/j.apcatb.2018.08.001.
[86] Esteve-Adell I, Bakker N, Primo A, Hensen EJM, García H. Chemistry 2017;2:6338–43. https://doi.org/10.1002/slct.201701138.
[87] Boudart M. Adv Catal 1969;20:153–66. https://doi.org/10.1016/S0360-0564(08)60271-0.
[88] Lehnert K, Claus P. Catal Commun 2008;9:2543–6. https://doi.org/10.1016/j.catcom.2008.07.002.
[89] Van Hardeveld R, Hartog F. Surf Sci 1969;15:189–230. https://doi.org/10.1016/0039-6028(69)90148-4.
[90] Wawrzetz A, Peng B, Hrabar A, Jentys A, Lemonidou AA, Lercher JA. J Catal 2010;269:411–20. https://doi.org/10.1016/j.jcat.2009.11.027.
[91] Barbelli ML, Pompeo F, Santori GF, Nichio NN. Catal Today 2013;213:58–64. https://doi.org/10.1016/j.cattod.2013.02.023.
[92] Kim Y, Kim M, Jeong H, Kim Y, Choi SH, Ham HC, Lee SW, Kim JY, Song KH, Yoon CW, Jo YS, Sohn H. High purity hydrogen production via aqueous phase reforming of xylose over small Pt nanoparticles on a γ-Al_2O_3 support. Int J Hydrogen Energy 2020;45:13848–61. https://doi.org/10.1016/j.ijhydene.2020.03.014.
[93] Chen A, Chen P, Cao D, Lou H. Int J Hydrogen Energy 2015;40:14798–805. https://doi.org/10.1016/j.ijhydene.2015.09.030.
[94] Yamaguchi W, Tai Y. Chem Lett 2014;43:313–5. https://doi.org/10.1246/cl.131014.
[95] Vikla AKK, Simakova I, Demidova Y, Keim EG, Calvo L, Gilarranz MA, He S, Seshan K. Appl Catal A Gen 2021;610. https://doi.org/10.1016/j.apcata.2020.117963.
[96] Callison J, Subramanian ND, Rogers SM, Chutia A, Gianolio D, Catlow CRA, Wells PP, Dimitratos N. Appl Catal B Environ 2018;238:618–28. https://doi.org/10.1016/j.apcatb.2018.07.008.
[97] Duarte HA, Sad ME, Apesteguía CR. Catal Today 2017;296:59–65. https://doi.org/10.1016/j.cattod.2017.04.067.
[98] Duarte HA, Sad ME, Apesteguía CR. Int J Hydrogen Energy 2017;42:4051–60. https://doi.org/10.1016/j.ijhydene.2016.11.119.
[99] Duarte HA, Sad ME, Apesteguía CR. Int J Hydrogen Energy 2016;41:17290–6. https://doi.org/10.1016/j.ijhydene.2016.07.071.
[100] Waheed A, Wang X, Maeda N, Naito S, Baiker A. Appl Catal A Gen 2019;581:111–5. https://doi.org/10.1016/j.apcata.2019.05.029.
[101] Zhao Z, Zhang L, Tan Q, Yang F, Faria J, Resasco D. AIChE J 2019;65:151–60. https://doi.org/10.1002/aic.16430.
[102] Van Haasterecht T, Swart M, De Jong KP, Bitter JH. J. Energy Chem. 2016;25:289–96. https://doi.org/10.1016/j.jechem.2016.01.006.
[103] Williams MF, Fonfé B, Sievers C, Abraham A, van Bokhoven JA, Jentys A, van Veen JAR, Lercher JA. J Catal 2007;251:485–96. https://doi.org/10.1016/j.jcat.2007.06.009.
[104] Ciftci A, Peng B, Jentys A, Lercher JA, Hensen EJM. Appl Catal A Gen 2012;431–432:113–9. https://doi.org/10.1016/j.apcata.2012.04.026.
[105] Shabaker JW, Huber GW, Davda RR, Cortright RD, Dumesic JA. Catal Lett 2003;88:1–8. https://doi.org/10.1023/A:1023538917186.
[106] Wen G, Xu Y, Ma H, Xu Z, Tian Z. Int J Hydrogen Energy 2008;33:6657–66. https://doi.org/10.1016/j.ijhydene.2008.07.072.
[107] Menezes AO, Rodrigues MT, Zimmaro A, Borges LEP, Fraga MA. Renew Energy 2011;36:595–9. https://doi.org/10.1016/j.renene.2010.08.004.
[108] Liu J, Sun B, Hu J, Pei Y, Li H, Qiao M. J Catal 2010;274:287–95. https://doi.org/10.1016/j.jcat.2010.07.014.
[109] Kim H, Ju H, Kim T, Jeong K, Chae H, Jeong S, Lee C, Kim C. Catal Today 2012;185:73–80. https://doi.org/10.1016/j.cattod.2011.08.012.
[110] Koichumanova K, Vikla AKK, Cortese R, Ferrante F, Seshan K, Duca D, Lefferts L. Appl Catal B Environ 2018;232:454–63. https://doi.org/10.1016/j.apcatb.2018.03.090.
[111] Stekrova M, Rinta-Paavola A, Karinen R. Catal Today 2018;304:143–52. https://doi.org/10.1016/j.cattod.2017.08.030.

[112] Li D, Li Y, Liu X, Guo Y, Pao CW, Chen JL, Hu Y, Wang Y. ACS Catal 2019;9:9671–82. https://doi.org/10.1021/acscatal.9b02243.
[113] Liu X, Guo Y, Xu W, Wang Y, Gong X, Guo Y, Guo Y, Lu G. Kinet Catal 2011;52:817–22. https://doi.org/10.1134/S0023158411060115.
[114] Ricote S, Jacobs G, Milling M, Ji Y, Patterson PM, Davis BH. Appl Catal A Gen 2006;303:35–47. https://doi.org/10.1016/j.apcata.2006.01.025.
[115] Iriondo A, Barrio VL, Cambra JF, Arias PL, Güemez MB, Navarro RM, Sánchez-Sánchez MC, Fierro JLG. Top Catal 2008;49:46–58. https://doi.org/10.1007/s11244-008-9060-9.
[116] Roy B, Sullivan H, Leclerc CA. J Power Sources 2014;267:280–7. https://doi.org/10.1016/j.jpowsour.2014.05.090.
[117] Wen G, Xu Y, Liu Q, Wang C, Liu H, Tian Z. Catal Lett 2011;141:1851–8. https://doi.org/10.1007/s10562-011-0712-1.
[118] Rahman MM, Church TL, Minett AI, Harris AT. ChemSusChem 2013;6:1006–13. https://doi.org/10.1002/cssc.201200797.
[119] Bastan F, Kazemeini M, Larimi A, Maleki H. Int J Hydrogen Energy 2018;43:614–21. https://doi.org/10.1016/j.ijhydene.2017.11.122.
[120] Jeon S, Roh HS, Moon DJ, Bae JW. RSC Adv 2016;6:68433–44. https://doi.org/10.1039/c6ra09522d.
[121] Ravenelle RM, Copeland JR, Kim W-G, Crittenden JC, Sievers C. Am. Chem. Soc. Catal. 2011;1:552–61. https://doi.org/10.1021/cs1001515.
[122] Ravenelle RM, Copeland JR, Van Pelt AH, Crittenden JC, Sievers C. Top Catal 2012;55:162–74. https://doi.org/10.1007/s11244-012-9785-3.
[123] Liu F, Okolie C, Ravenelle RM, Crittenden JC, Sievers C, Bruijnincx PCA, Weckhuysen BM. Appl Catal A Gen 2018;551:13–22. https://doi.org/10.1016/j.apcata.2017.11.025.
[124] Van Cleve T, Underhill D, Veiga Rodrigues M, Sievers C, Medlin JW. Langmuir 2018;34:3619–25. https://doi.org/10.1021/acs.langmuir.8b00465.
[125] Goma D, Delgado JJ, Lefferts L, Faria J, Calvino JJ, Cauqui MÁ. Nanomaterials 2019;9. https://doi.org/10.3390/nano9111582.
[126] Bastan F, Kazemeini M, Larimi AS. Renew Energy 2017;108:417–24. https://doi.org/10.1016/j.renene.2017.02.076.
[127] Jeon S, Ham H, Suh YW, Bae JW. RSC Adv 2015;5:54806–15. https://doi.org/10.1039/c5ra07124k.
[128] Larimi AS, Kazemeini M, Khorasheh F. Appl Catal A Gen 2016;523:230–40. https://doi.org/10.1016/j.apcata.2016.05.028.
[129] Harju H, Pipitone G, Lefferts L. Front. Chem. 2020;8. https://doi.org/10.3389/fchem.2020.00017.
[130] Kaya B, Irmak S, Hasanoglu A, Erbatur O. Int J Hydrogen Energy 2014;39:10135–40. https://doi.org/10.1016/j.ijhydene.2014.04.180.
[131] Wang X, Li N, Webb JA, Pfefferle LD, Haller GL. Appl Catal B Environ 2010;101:21–30. https://doi.org/10.1016/j.apcatb.2010.08.028.
[132] Meryemoglu B, Irmak S, Hasanoglu A, Erbatur O, Kaya B. Fuel 2014;134:354–7. https://doi.org/10.1016/j.fuel.2014.05.067.
[133] Kim H, Kim T, Ju H, Jeong K, Chae H, Jeong S, Lee C, Kim C. Int J Hydrogen Energy 2012;37:12187–97. https://doi.org/10.1016/j.ijhydene.2012.05.126.
[134] De Jong KP. Synthesis of solid catalysts. 2009. https://doi.org/10.1002/9783527626854.
[135] Tanksale A, Zhou CH, Beltramini JN, Lu GQ. J Inclusion Phenom Macrocycl Chem 2009;65:83–8. https://doi.org/10.1007/s10847-009-9618-6.
[136] Cesar DV, Santori GF, Pompeo F, Baldanza MA, Henriques CA, Lombardo E, Schmal M, Cornaglia L, Nichio NN. Int J Hydrogen Energy 2016;41:22000–8. https://doi.org/10.1016/j.ijhydene.2016.07.168.
[137] Lemus J, Bedia J, Calvo L, Simakova IL, Murzin DY, Etzold BJM, Rodriguez JJ, Gilarranz MA. Catal. Sci. Technol. 2016;6:5196–206. https://doi.org/10.1039/c6cy00403b.
[138] El Doukkali M, Iriondo A, Arias PL, Requies J, Gandarías I, Jalowiecki-Duhamel L, Dumeignil F. Appl Catal B Environ 2012;125:516–29. https://doi.org/10.1016/j.apcatb.2012.06.024.
[139] El Doukkali M, Iriondo A, Cambra JF, Jalowiecki-Duhamel L, Mamede AS, Dumeignil F, Arias PL. J Mol Catal A Chem 2013;368–369:125–36. https://doi.org/10.1016/j.molcata.2012.12.006.
[140] El Doukkali M, Iriondo A, Cambra JF, Arias PL. Recent improvement on H2 production by liquid phase reforming of glycerol: catalytic properties and performance, and deactivation studies. Top Catal 2014:1066–77. https://doi.org/10.1007/s11244-014-0271-y.
[141] El Doukkali M, Iriondo A, Cambra JF, Gandarias I, Jalowiecki-Duhamel L, Dumeignil F, Arias PL. Appl Catal A Gen 2014;472:80–91. https://doi.org/10.1016/j.apcata.2013.12.015.
[142] Roy B, Leclerc CA. J Power Sources 2015;299:114–24. https://doi.org/10.1016/j.jpowsour.2015.08.069.
[143] Roy B, Martinez U, Loganathan K, Datye AK, Leclerc CA. Int J Hydrogen Energy 2012;37:8143–53. https://doi.org/10.1016/j.ijhydene.2012.02.056.
[144] Roy B, Artyushkova K, Pham HN, Li L, Datye AK, Leclerc CA. Int J Hydrogen Energy 2012;37:18815–26. https://doi.org/10.1016/j.ijhydene.2012.09.098.
[145] Yun YS, Park DS, Yi J. Catal Sci Technol 2014;4:3191–202. https://doi.org/10.1039/c4cy00320a.
[146] Morales-Marín A, Ayastuy JL, Iriarte-Velasco U, Gutiérrez-Ortiz MA. Appl Catal B Environ 2019;244:931–45. https://doi.org/10.1016/j.apcatb.2018.12.020.
[147] Delgado SN, Yap D, Vivier L, Especel C. J Mol Catal A Chem 2013;367:89–98. https://doi.org/10.1016/j.molcata.2012.11.001.
[148] El Doukkali M, Iriondo A, Miletic N, Cambra JF, Arias PL. Int J Hydrogen Energy 2017;42:23617–30. https://doi.org/10.1016/j.ijhydene.2017.04.218.
[149] Irmak S, Meryemoglu B, Ozsel BK, Hasanoglu A, Erbatur O. Int J Hydrogen Energy 2015;40:14826–32. https://doi.org/10.1016/j.ijhydene.2015.09.010.
[150] Keshavarz A, Salabat A. Chemistry 2019;4:6094–100. https://doi.org/10.1002/slct.201900376.
[151] Soleimani S, Salabat A, Tabor RF. J Colloid Interface Sci 2014;426:287–92. https://doi.org/10.1016/j.jcis.2014.03.033.
[152] Biausque GM, Laveille PV, Anjum DH, Zhang B, Zhang X, Caps V, Basset JM. ACS Appl Mater Interfaces 2017;9:30643–53. https://doi.org/10.1021/acsami.7b08201.
[153] Roy B, Loganathan K, Pham HN, Datye AK, Leclerc CA. Int J Hydrogen Energy 2010;35:11700–8. https://doi.org/10.1016/j.ijhydene.2010.07.167.
[154] Ciftci A, Eren S, Ligthart DAJM, Hensen EJM. ChemCatChem 2014;6:1260–9. https://doi.org/10.1002/cctc.201301096.
[155] Lange JP. Catal Sci Technol 2016;6:4759–67. https://doi.org/10.1039/c6cy00431h.
[156] Koichumanova K, Vikla AKK, De Vlieger DJM, Seshan K, Mojet BL, Lefferts L. ChemSusChem 2013;6:1717–23. https://doi.org/10.1002/cssc.201300445.
[157] Esteve-Adell I, Bakker N, Primo A, Hensen E, García H. ACS Appl Mater Interfaces 2016;8:33690–6. https://doi.org/10.1021/acsami.6b11904.
[158] Saleheen M, Heyden A. ACS Catal 2018;8:2188–94. https://doi.org/10.1021/acscatal.7b04367.

[159] Soták T, Hronec M, Vávra I, Dobročka E. Int J Hydrogen Energy 2016;41:21936–44. https://doi.org/10.1016/j.ijhydene.2016.08.183.
[160] Ahmadi M, Mistry H, Roldan Cuenya B. J Phys Chem Lett 2016;7:3519–33. https://doi.org/10.1021/acs.jpclett.6b01198.
[161] Zoppi G, Pipitone G, Galletti C, Rizzo AM, Chiaramonti D, Pirone R, Bensaid S. Catal Today 2021;365:206–13. https://doi.org/10.1016/j.cattod.2020.08.013.
[162] Zoppi G, Pipitone G, Pirone R, Bensaid S. Catal Today 2021. https://doi.org/10.1016/j.cattod.2021.06.002.
[163] Khodabandehloo M, Larimi A, Khorasheh F. Energy Convers Manag 2020;225:113483. https://doi.org/10.1016/j.enconman.2020.113483.
[164] Kayfeci M, Kecebaş A, Bayat M. Hydrogen production. In: Calise F, D'accadia MD, Santarelli M, Lanzini A, Ferrero D, editors. Sol. Hydrog. Prod. Elsevier Inc.; 2019. p. 45–83. https://doi.org/10.1016/B978-0-12-814853-2.00003-5.
[165] Sladkovskiy DA, Godina LI, Semikin KV, Sladkovskaya EV, Smirnova DA, Murzin DY. Chem Eng Res Des 2018;134:104–16. https://doi.org/10.1016/j.cherd.2018.03.041.